Journal Pre-proof

Primary production dynamics on the Agulhas Bank in autumn

Alex J. Poulton, Sixolile L. Mazwane, Brian Godfrey, Filipa Carvalho, Edward Mawji, Juliane U. Wihsgott, Margaux Noyon

PII: S0967-0645(22)00138-2

DOI: https://doi.org/10.1016/j.dsr2.2022.105153

Reference: DSRII 105153

To appear in: *Deep-Sea Research Part II*

Received Date: 22 June 2021

Revised Date: 1 July 2022

Accepted Date: 12 July 2022

Please cite this article as: Poulton, A.J., Mazwane, S.L., Godfrey, B., Carvalho, F., Mawji, E., Wihsgott, J.U., Noyon, M., Primary production dynamics on the Agulhas Bank in autumn, *Deep-Sea Research Part II* (2022), doi: https://doi.org/10.1016/j.dsr2.2022.105153.

Author contributions

Alex J Poulton: Funding acquisition, Conceptualization, Investigation, Formal analysis, Writing – original draft, Writing – review and editing; **Sixolile L Mazwane:** Conceptualization, Investigation, Formal analysis, Writing – review and editing; **Brian Godfrey:** Data curation, Investigation, Formal analysis, Writing – review and editing; **Filipa Carvalho:** Data curation, Investigation, Formal analysis, Writing – review and editing; **Juliane Wihsgott:** Data curation, Investigation, Formal analysis, Writing – review and editing; **Edward Mawji:** Data curation, Investigation, Formal analysis, Writing – review and editing; **Margaux Noyon:** Conceptualization, Investigation, Formal analysis, Writing – original draft, Writing – review and editing.

Primary production dynamics on the Agulhas Bank in autumn

Alex J. Poulton[a,*], Sixolile L. Mazwane[b], Brian Godfrey[b], Filipa Carvalho[c], Edward Mawji[c], Juliane U. Wihsgott[d], Margaux Noyon[b]

[a] *The Lyell Centre for Earth and Marine Science and Technology, Heriot-Watt University, Edinburgh, EH14 4AS, UK*

[b] *Nelson Mandela University, Gqeberha, 6001, South Africa*

[c] *National Oceanography Centre, Southampton, SO14 3ZH, UK*

[d] *National Oceanography Centre, Liverpool, L69 3GP, UK*

* Corresponding author. *Lyell Centre, Heriot-Watt University, Edinburgh, EH14 4AS, UK*

E-mail address: a.poulton@hw.ac.uk (A.J. Poulton).

Highlights:

- Net primary production (NPP) ranged from 0.3 to 1.1 g C m^{-2} d^{-1} during March on the Agulhas Bank.
- Surface mixed layers on the bank had abundant irradiance and nitrate to support NPP rates.
- Subsurface chlorophyll maxima (SCM) occurred at 47% of sites, containing 1.7 to 10.3 mg m^{-3}.
- SCM deepened east-to-west, linked to in-situ growth (east) and photo-acclimation (west).

ABSTRACT

The Agulhas Bank is a productive shelf sea, supporting important fish stocks, nursery grounds, and spawning sites. Few studies have examined the dynamics of primary production and the physio-chemical conditions that support this productivity during autumn. We report from a 14-day, 51-station survey of the central and eastern (21-27°E) Agulhas Bank in March 2019, during which we examined water-column structure, macronutrients, chlorophyll-*a* (total and size-fractionated), diatom cell counts and Net Primary Production (NPP). East to west trends were observed, with surface mixed layers (SML) and stratification increasing to the west. Euphotic zones were deeper than the SML, with SML irradiance conditions indicative of favorable light conditions for NPP. On average, surface waters contained ~1.2 µmol N L^{-1} of nitrate (nitrate+nitrite; NO_3) and ~3 µmol Si L^{-1} of silicic acid, which contrasts with nutrient deficient subtropical source waters. Surface chlorophyll-*a* ranged from 0.3 to 5.1 mg m^{-3}, with high values inshore and near the shelf break. Nanoplankton (2-20 µm) dominated size-fractionated chlorophyll-*a*, with microplankton contributions increasing to the west. Measurements of NPP were collected at seven stations, ranging from 0.3 to 1.1 g C m^{-2} d^{-1}, with a statistically significant relationship between integrated NPP and surface chlorophyll-*a* allowing further estimates of NPP (0.1 to 1.1 g C m^{-2} d^{-1}). We estimated nitrogen-demand to support NPP, with a comparison to surface NO_3 indicating ample nutrients to support daily NPP. Around half of the stations possessed a Subsurface Chlorophyll Maximum (SCM), with chlorophyll-*a* ranging from 1.7 to 10.3 mg m^{-3}. Characteristics of the SCM (depth, light level, chlorophyll-to-carbon ratios) showed east to west variability, implying that the mechanisms of SCM formation ranged from in-situ growth (east) to photo-acclimation (west).

Keywords: Phytoplankton; upwelling; western boundary current; shelf sea.

1. Introduction

Autumn represents a key period of marine production in temperate and high-latitude shelf seas (Wihsgott et al., 2019), with shelf seas annually representing ~10 to 30% of global primary production (Field et al., 1998) and high proportions of global carbon sequestration, despite representing less than 10% of the ocean area (Bauer et al., 2013). Coastal waters are key sites for phytoplankton growth and primary production, and the organic matter produced by these phytoplankton communities fuels marine ecosystems. Due to the high rates of primary and secondary production associated with shelf seas, they also play host to economically important fisheries and support ~90% of global fish catches (Pauly et al., 2002).

The Agulhas Bank is considered a productive shelf sea, with surface chlorophyll-*a* (Chl*a*) concentrations often greater than 2 mg m^{-3}, and supports major spawning grounds for commercially important marine species (e.g., Agulhas sole, Cape anchovy, chokka squid, hake and kingklip) (Boyd et al., 1992; Hutchings, 1994; Probyn et al., 1994; Hutchings et al., 2002). Applying the Vertically Generalized Production Model (VGPM) to estimate Net Primary Production (NPP) from satellite data, Mazwane et al. (this issue) found that monthly mean productivity on the central and eastern Agulhas Bank (33-37°S, 21-28°E; Fig. 1) was relatively high all year-round (1998-2018 average ± standard deviation: 1.4 ± 0.4 g C m^{-2} d^{-1}), with little seasonality compared to other temperate shelf seas. These observations agree with a previous satellite-chlorophyll based study using a broad-band light transmission model to estimate NPP on the Agulhas Bank by Demarcq et al. (2008) (1997-2003 average: 1.2 g C m^{-2} d^{-1}).

With an annual magnitude of variability in satellite-derived Chl*a* of only ~1 mg m^{-3} (from 0.5-1.5 mg m^{-3}; see also: Demarcq et al., 2003; Lamont et al., 2018), despite seasonal changes in Photosynthetically Available Radiation (PAR) of 20 to 60 mol photons m^{-2} d^{-1} and a seasonal temperature range of ~5°C, the Agulhas Bank sustains high levels of annual NPP (in-situ estimates: 681 g C m^{-2} yr^{-1}, Brown et al., 1991; 656 g C m^{-2} d^{-1}, Probyn et al., 1994; satellite estimates: 438 g C m^{-2} yr^{-1}, Demarcq et al., 2008; 514 g C m^{-2} yr^{-1}, Mazwane et al., this issue). High NPP occurs in late spring and early summer (November-December), with lower NPP in autumn (March-May) and lowest NPP in winter (June-July), although the amplitude of seasonal variability is only ~0.5 to 1.0 g C m^{-2} d^{-1} (Demarcq et al., 2008; Mazwane et al., this issue). To sustain such relative seasonal stability and high annual NPP, which is higher than global averages for most shelf systems (e.g. 385 g C m^{-2} yr^{-1}, Longhurst et al., 1995), the Agulhas Bank must have efficient and seasonally stable nutrient supplies and recycling mechanisms.

In many temperate shelf seas, the phenology of primary production is dominated by a spring bloom, triggered by stratification and optimum light conditions (Hopkins et al., 2021), with weaker rates during the stratified summer, which is then terminated by increased autumn mixing (Wihsgott et al., 2019). During summer, phytoplankton adapt to low surface nutrients and low light at the base of the surface mixed layer (SML), forming a subsurface chlorophyll maximum (SCM) at the thermocline to take advantage of vertical fluxes of

inorganic nutrients from bottom waters (Holligan et al., 1984a; Carter et al., 1987; Sharples et al., 2001; Hickman et al., 2012; Cullen, 2015). Phytoplankton in the SCM adapt to the low light levels by increasing cellular pigmentation, which leads to increases in chlorophyll-to-carbon (Chl:C) ratios (Geider et al., 1998; Cullen, 2015). The SCM can represent a maximum in terms of NPP through a combination of in-situ growth, elevated nutrient fluxes, and high light availability (Cullen, 1982, 2015). Weakening stratification in autumn is often associated with a secondary peak in biomass, considered an 'autumn bloom', which may reflect elevated production and/or the redistribution of SCM material (Painter et al., 2016; Wihsgott et al., 2019). On the Agulhas Bank, a lack of pronounced spring peaks (September-October) in Chl*a* or NPP, with high levels seen from spring through to late summer, with only a moderate peak in autumn (Demarcq et al., 2008; Lamont et al., 2018; Mazwane et al., this issue), implies that the phenology of marine production on the Bank responds differently to other shelf seas.

The Agulhas Current, one of the strongest western boundary currents, flows close to the shelf break of the Agulhas Bank, carrying large amounts of warm (>18^{o}C), saline and relatively nutrient-poor water from the Indian Ocean (Goschen et al., 2012; Lutjeharms, 2006). Subtropical surface water from the Agulhas Current helps to form the surface waters on the Agulhas Bank, with low concentrations of nitrate (2-8 µmol N L^{-1}), phosphate (0.2-0.8 µmol P L^{-1}) and silicic acid (<2 µmol Si L^{-1}) (Lutjeharms et al., 1996). As the Agulhas Current moves along the shelf break, it drives cold (6-14^{o}C), nutrient-rich deeper waters (South Indian Ocean Central Water; Lutjeharms et al., 1996; Lutjeharms, 2006) onto the shelf (Largier and Swart, 1987; Swart and Largier, 1987; Chapman and Largier, 1989; Jackson et al., 2012; Malan et al., 2018). Relative to surface waters, South Indian Ocean Central Water has elevated nutrients concentrations of 8 to 18 µmol N L^{-1} of nitrate, 0.8 to 2.0 µmol P L^{-1} of phosphate and 4 to 7 µmol Si L^{-1} of silicic acid (Lutjeharms et al., 1996). Subsequent upwelling of this deep nutrient-rich water to the surface supports NPP on the bank (Hutchings, 1994; Jackson et al., 2012) and contributes to the Agulhas Bank being more biologically productive than many other shelf systems (Probyn et al., 1994; Lutjeharms, 2007).

Advection of these cold, deep waters onto the Agulhas Bank exhibits seasonality, related to seasonal changes in stratification and Agulhas Current speed (Hutchinson et al., 2018) and is key to the formation and maintenance of a strong thermocline across the bank (Largier and Swart, 1987; Swart and Largier, 1987). The relationship between the Agulhas Bank and the Agulhas Current is complex, with various meanders (e.g. Natal Pulses) and eddies that may intrude onto the bank (Boyd and Shillington, 1994; Lutjeharms, 2006; Jackson et al., 2012; Malan et al., 2018), with a concomitant export of material off the shelf (Jackson et al., 2012). While the general current direction on the bank is westwards (Jackson et al., 2012), meanders of the Agulhas Current onto the shelf can alter or even reverse the surface currents (Lutjeharms, 2006).

The Agulhas Bank experiences several different types of upwelling of deep nutrient-rich water to support elevated annual NPP: (a) upwelling at the shelf edge via interactions between the shelf break and the Agulhas Current; (b) meander-induced upwelling on the inshore side of the Agulhas Current; and (c) wind-driven

upwelling in near-shore coastal waters (Chapman and Largier, 1989; Boyd and Shillington, 1994; Probyn et al., 1994; Jackson et al., 2012; Lutjeharms, 2006; Lutjeharms et al., 1996; Malan et al., 2018; Swart and Largier, 1987). Unlike the shelf break, the inner coastal waters of the Agulhas Bank, dominated by capes and headlands, are strongly wind-driven (Schumann et al., 1982), with westerlies dominant throughout the year, while summer and autumn are associated with increased easterly wind events (Hutchings, 1994; Schumann et al., 1982) which support localised coastal upwelling of nutrient-rich shelf waters (Boyd and Shillington, 1994; Lutjeharms et al., 1996; Lutjeharms, 2006).

Water-columns on the Agulhas Bank exhibit steep vertical temperature and density gradients, with strong vertical transitions in temperature (up to 1-2^{o}C m^{-1}) leading to strong stratification of the water column (Carter et al., 1987; Largier and Swart, 1987). The thermocline on the Agulhas Bank is formed and maintained through the combined processes of coastal upwelling, advection of warm surface and cold deep waters from the Agulhas Current, and surface water heating (Largier and Swart, 1987; Swart and Largier, 1987; Lutjeharms, 2006). Strong stratification of the water-column on the Agulhas Bank exerts a significant control on the availability of nutrients to surface waters away from coastal and shelf-break upwelling locations, and is associated with widespread SCM (Probyn et al., 1994; Lutjeharms et al., 1996). These SCM on the bank are considered light limited features, important for zooplankton feeding and the spawning success of local fish populations (Carter et al., 1987; Verheye et al., 1994).

To further understand the phytoplankton dynamics during autumn on the central and eastern Agulhas Bank, we undertook a 14-day research cruise sampling from east to west across the bank (Fig. 1). Our objectives were to: (1) investigate in-situ rates of daily NPP; (2) explore the potential limiting factors for NPP (light, nutrients, grazing); and (3) analyze the distribution and characteristics of SCM. When examining the SCM on the Agulhas Bank, our specific research question related to whether the SCM represented a deep peak in NPP, as observed by other studies on the Bank (Carter et al., 1987; Probyn et al., 1994; Barlow et al., 2010), as well as to explore the factors involved in its formation and maintenance.

2. Methods

2.1. Sampling

Sampling occurred on the central and eastern Agulhas Bank onboard the *RV Ellen Khuzwayo* (cruise EK188, 21 March to 2 April 2019; Noyon, 2019) along several inshore-offshore transects from east to west (Fig. 1). During the cruise, 51 stations were sampled over a 7-day survey (23 to 30 March) through deployment of a Seabird 911+ V2 CTD system with rosette sampler equipped with twelve 8 L Niskin bottles (OTE: Ocean Test Equipment). Processing and calibration of CTD data followed standard procedures and are detailed in Noyon (2019).

At all 51 stations the CTD system was deployed to measure full depth vertical profiles of temperature, salinity, density, chlorophyll-fluorescence, and oxygen. Discrete water samples were collected from all stations (n = 51) from 6 to 12 depths (depending on water depth) for determination of macronutrient concentrations (nitrate+nitrite [NO_3], phosphate [PO_4], silicic acid [$Si(OH)_4$]). Water samples from a smaller number of stations and depths were collected for the analysis of phytoplankton biomass (total Chl*a*; n = 34, 6 depths), community composition (size-fractionated Chl*a* (n = 32, 6 depths), phytoplankton cell counts (n = 29, 2 depths), and the composition of particulate material (n = 29, 6 depths; particulate organic carbon [POC], particulate nitrogen [PN], biogenic silica [$bSiO_2$])). At a limited number of stations (n = 7), measurements of daily NPP (dawn to dawn) were made using the tracer ^{13}C. Location of the productivity stations was determined by the pre-dawn sampling location each day of the survey.

Transects were numbered from 1 to 12 from east to west (Fig. 1), and sequentially from inshore (e.g. 1.1, 5.1, 7.1) to offshore waters near the shelf break (e.g. 1.4, 5.5, 12.6). A repeat was done for station 9.1, termed 9.1b, due to sudden bad weather, with 9.1b slightly to the east of 9.1 (see Fig. 1). A number of mooring stations were also visited during the cruise, with one station (CR4) sampled as part of the grid survey to the northeast of station 10.5 (see Fig. 1).

Depth of the surface mixed layer (SML) was determined from density profiles from the CTD, by identifying where potential density increased by 0.125 kg m^{-3} above the surface (5 m) value (Hopkins et al., 2021) and density profiles were visually checked. An alternative expression of the SML and pycnocline was examined in terms of the vertical buoyancy frequency (Brunt-Väisälä frequency, N^2), with the depth of its maximum value (Carvalho et al., 2017) showing good agreement in most cases to the SML depth (see Supplementary Fig. S1), with some notable exceptions (see Results). Bottom mixed layer (BML) depth was defined as an 0.02 kg m^{-3} decrease in potential density from the deepest value (Hopkins et al., 2021) and BML thickness was determined as the difference between BML depth and bottom depth (i.e., in our case the deepest CTD depth).

Fluorescence from the CTD was calibrated against discrete measurements of Chl*a* (see Section 2.2) using a linear regression (r = 0.859, p<0.001, n = 167; FChl = (Fl - 0.07) * 14.47, where Fl is the raw CTD fluorescence) (Noyon, 2019). Comparison of day and nighttime surface values showed no consistent pattern of quenching of surface fluorescence signals, with variability between CTD-fluorescence and discrete Chl*a* during both day and night. Vertical profiles of calibrated CTD-fluorescence (FChl) were examined to determine the value and depth of maximum Chl*a* concentration in each profile. A rigid definition for the SCM was adopted to attempt to identify stations which had well-defined SCM rather than just variable vertical FChl profiles. In this case, SCM were identified as being present when SCM FChl values were 1.5-times greater than surface FChl values, and this definition identified SCM at 24 of the 51 stations sampled. It is possible that other stations had weak SCM present (i.e. <50% increase from surface Chl*a*), but a conservative approach was preferred to avoid misinterpretation of phytoplankton dynamics across the Agulhas Bank.

A LI-COR Biospherical PAR Sensor on the CTD was used to determine downwelling irradiance and the vertical attenuation coefficient of PAR ($K_{d(PAR)}$, m^{-1}) during daytime CTD casts using the relationship describing the exponential decline of downwelling irradiance with depth (Kirk, 1983). For night-time casts, $K_{d(PAR)}$ was estimated from a cruise-specific relationship between surface FChl and $K_{d(PAR)}$ (linear regression; $K_{d(PAR)} = 0.109 + 0.0185\text{FChl}$; $r = 0.71$, $n = 27$, $p<0.001$). Depth of the euphotic zone (Z_{eup}) was calculated as the depth to which 1% surface irradiance penetrates. Average SML irradiance ($\bar{E}_{SML}$), which describes the mean irradiance experienced by a particle mixed within the mixed layer, was determined following Poulton et al. (2011) using a combination of K_d and SML.

2.2. Total and size-fractionated chlorophyll-a

Total Chl*a* concentrations (mg m^{-3}) were measured on 0.2 L water samples filtered onto 25 mm Fisherbrand MF300 glass-fibre filters. Size-fractionated Chl*a* (fractions: 0.2-2, 2-20, >20 µm) was determined through sequential gravity filtering 0.2 L water samples through 20 µm and 2 µm 47 mm Nucleopore filters, and then through a 0.2 µm 47 mm Nucleopore filter under gentle vacuum. All filters were extracted in 6 mL 90% acetone (Sigma-Aldrich, UK) at 4°C for 18 to 24 hr, with Chl*a* fluorescence then measured on a Turner Designs Trilogy™ fluorometer using a non-acidification module (after Welschmeyer, 1994) calibrated with solid and pure Chl*a* standards (Sigma-Aldrich, UK).

2.3. Macronutrient concentrations

Water samples for macronutrient concentrations were collected into acid-cleaned 50 mL HDPE bottles, which were immediately frozen (-20°C) onboard and kept frozen until analysis. Concentrations (µmol L^{-1}) of nitrate+nitrite (NO_3), phosphate (PO_4) and silicic acid ($Si(OH)_4$) were measured with a SEAL QuAAtro39 auto-analyzer following standard protocols (Becker et al., 2020). Certified reference materials were used daily (KANSO, Japan) and analytical procedures followed International GO-SHIP recommendations (Becker et al., 2021). The typical uncertainty of the analytical results were between 0.5% and 1%, and the limits of detection for nitrate and phosphate were 0.02 µmol L^{-1}, while $Si(OH)_4$ was always higher than the detection limit (0.05 µmol Si L^{-1}). Deficiencies of NO_3 relative to PO_4 and $Si(OH)_4$ were described relative to the Redfield (1958) ratio with N* (= NO_3 - (16 x PO_4); Moore et al., 2009) and relative to the 1:1 ratio of $Si(OH)_4$ to NO_3 uptake in diatoms (Brzezinski, 1985) through Si* (= $Si(OH)_4$ - NO_3; Bibby and Moore, 2011).

2.4. Net primary production

Daily rates (dawn to dawn, 24 h) of net primary production (NPP) were determined using the ^{13}C stable isotope method (Legendre and Gosselin, 1996) following Daniels et al. (2015). Water samples were collected from 6 depths for 5 stations, 3 depths for 1 station (5.1) and 1 depth (55% depth) for 1 station (9.1b). In the case of the station with samples from 3 depths (5.1), these included the depths of 55, 4.5 and 1% incidental

irradiance, while stations with 6 depths included the depths of 55%, 33%, 20%, 7%, 4.5%, and 1% of incidental irradiance. Sampling depths were determined by estimating that the bottom of the SML occurred at the 4.5% irradiance level and the $K_{d(PAR)}$ back-calculated.

Water samples were collected from the six depths in 1.2 L polycarbonate (Nalgene™) bottles and inoculated with 500 µmol L^{-1} of ^{13}C labelled sodium bicarbonate, representing ~11% of the ambient dissolved inorganic carbon pool (assumed to be ~2318 µmol C L^{-1}). Samples were incubated in on-deck incubators, chilled with sea surface water, and light depths were replicated using combinations of optical filters (misty-blue and neutral density, LEE™ Filters) after Poulton et al. (2013). Incubations were terminated after 24 h by filtration onto pre-ashed (>400°C, >4 h) Fisherbrand MF300 glass-fibre filters. Acid-labile particulate inorganic carbon (PIC) was removed by adding a few drops of 1% HCl to the filter followed by extensive rinsing with freshly filtered (Whatman GFF) unlabelled seawater (Daniels et al., 2015). Filters were oven dried (40 °C, 8-12 h) and stored in cryotubes. A parallel 55% E_0 bottle for size-fractionated NPP (<20 µm) was also incubated, with the incubation terminated by pre-filtration through 20 µm polycarbonate (Nucleopore™) filters and the filtrate subsequently filtered as above. Isotopic analysis was performed on an automated nitrogen and carbon analysis preparation system with a 20-20 stable isotope analyser (PDZ Europa Scientific Instruments). The ^{13}C-fixation rate were calculated using the equations described in Legendre and Gosselin, (1996). The >20 µm NPP fraction was calculated as the difference between total NPP and <20 µm NPP.

2.5. Particulate biogenic silica ($bSiO_2$), particulate organic carbon (POC) and nitrogen (PN)

Particulate silica concentrations ($bSiO_2$; µmol Si kg^{-1}) were made on 0.5 L water samples filtered onto 0.8 µm polycarbonate (Nucleopore™) filters, rinsed with pH-adjusted MilliQ (pH >8), oven-dried at 40 to 50ºC for 10 to 12 h and stored in 15 mL HDPE tubes. For analysis, filters were digested in 0.2 M NaOH at 85ºC for 1 h, neutralized with 0.2 M HCl (Ragueaneau and Tréguer, 1994) and analyzed on a SEAL analytical AACE 7.03 autoanalyzer using standard techniques. Measurements of particulate organic carbon (POC) and nitrogen (PN) were made by filtering seawater samples (1 L) onto pre-ashed (>450ºC, >4 h) 25 mm MF300 Fisherbrand™ filters. Acid-labile particulate inorganic carbon (PIC) was removed by adding a few drops of 1% HCl to the filter followed by extensive rinsing with freshly filtered (Whatman GFF) unlabelled seawater (Daniels et al., 2015). The filters were then oven dried at 40 to 50ºC for 10 to 12 h, stored dry and analyzed using the same equipment as for ^{13}C analysis.

2.6. Phytoplankton enumeration

For phytoplankton enumeration, 100 mL water samples were preserved with acidic Lugol's solution (2% final solution) in 100 mL amber glass bottles. Diatom cells were counted in 50 mL Hydro-Bios chambers after a 24 to 48 h settling period using a Zeiss AxioObserver A1 inverted microscope (magnification X200).

3. Results

3.1. Water column structure

The depth of the SML in autumn showed an east to west deepening, from <10 m in the east to >20 m in the west (Fig. 2a), though the deepest SML across the Agulhas Bank was only 27 m (average ± standard deviation: 15 ± 5 m). Deepening of the SML was related to warming of the SML, with sea-surface (<5 m) temperatures generally warming from east to west (Fig. 2b). There were no clear or consistent inshore-offshore trends in depth or temperature of the SML. In March 2019, surface water temperatures ranged from 17 to 22°C (Fig. 2b; average: 20 ± 1°C), with salinities ranging from 34.7 to 35.3 (Table S1).

Vertical density profiles were also assessed in terms of buoyancy frequency (Brunt-Väisälä frequency, N^2), with the depth of the maximum buoyancy frequency compared to the SML depth and the maximum value of the buoyancy frequency used as information of the degree of stratification in the water column (Carvalho et al., 2017). The depth of the maximum buoyancy frequency showed the same strong east to west deepening as the SML depth (Figs. 2a and 2c). The value of the maximum buoyancy frequency also showed an east to west strengthening trend (Fig. 2d), from values of $<4 \times 10^3$ s^{-2} in the east to values $\sim 5 \times 10^3$ s^{-2} in the west. Increasing stratification from east to west likely relates to warming of sea-surface waters (Fig. 2b), as well as other physical factors related to widening of the shelf and interactions with the Agulhas Current.

The depth of the BML ranged from 23 to 271 m across the Agulhas Bank (Fig. 2e), with deepening of the BML from <50 m to >100 m from inshore to offshore stations as bottom depth also deepened. BML thickness showed a clear east to west trend with generally much wider BML in the west (>30 m) than in the east (<30 m) (Fig. 2f). The range of BML temperatures and salinities was 8 to 14°C and 34.7 to 35.2 (Table S1), respectively, which corresponds with the reported temperature and salinity range for South Indian Ocean Central Water (i.e., ~6-14°C, ~34.6-35.2; Fig. S2; Swart and Largier, 1987; Chapman and Largier, 1989).

3.2. Light regime

Measured values for $K_{d(PAR)}$ ranged from 0.09 to 0.20 m^{-1} (average: 0.14 ± 0.03 m^{-1}) for daytime CTD casts, with estimated $K_{d(PAR)}$ values from surface CTD calibrated-fluorescence Chl*a* measurements (see Methods) ranging from 0.12 to 0.20 m^{-1} (average: 0.15 ± 0.02 m^{-1}). Euphotic zone depths, here defined as the depth of penetration of 1% of surface irradiance (E_0) ranged from 18 to 62 m (average: 33 ± 8 m), with no clear east to west or inshore-offshore trend (Fig. 3a). During autumn, none of the sampling stations had euphotic zones shallower than the SML, with euphotic zone to SML ratios between 1 and 8. Estimates of the average irradiance in the SML ($\bar{E}_{SML}$; Fig. 3b) indicate that particles (e.g. phytoplankton) in Agulhas Bank SMLs during March received 26 to 76% of incidental irradiance (average: 44 ± 12%). An east to west trend of declining $\bar{E}_{SML}$ was observed, with SML for the Agulhas Bank east of 25°E having values greater than 60% of incidental irradiance (E_0) while values to the west (<25°E) were generally less than 40% of incidental irradiance (Fig. 3b).

3.3. Nutrient regime

Average SML NO_3 concentrations ranged from 0.1 to 6.2 µmol N L^{-1} (average: 1.2 ± 1.4 µmol N L^{-1}) across the Agulhas Bank in autumn, with generally similar concentrations in the east and west (Fig. 3c). High average SML values (>4-6.2 µmol N L^{-1}) were found at several offshore stations along transects 5, 6 and 7 (Fig. 3c). Average SML PO_4 concentrations ranged from 105 to 522 nmol P L^{-1} (average: 233 ± 97 nmol P L^{-1}), with a similar east to west declining trend (Table S1) and a significant (p<0.005) correlation with NO_3 (Pearson's product moment, r = 0.90, n =51).

Average SML NO_3 and PO_4 concentrations are similar to values previously reported for Subtropical Surface Water (see Fig. S2) (NO_3 2-8 µmol N L^{-1}, PO_4 200-800 nmol P L^{-1}; Lutjeharms et al., 1996) associated with the Agulhas Current. The relative concentration of SML average NO_3 to PO_4, represented here by N*, was negative at all sites, ranging from -1.6 to -5.2 (average: -2.5 ± 0.7) (Fig. 3d) and is indicative of 'nitrate-depletion' relative to phosphate on the Agulhas Bank in March. These N* values are in close agreement with N* estimated for the source waters of the Agulhas Bank, using values from Lutjeharms et al. (1996) (calculated N* range: -1.2 to -4.8, median N* -3.0), highlighting depleted nitrate (relative to phosphate) of subtropical source waters (see Fig. S2) for the Bank. Strongly negative N* values, less than -3.0, were limited to inshore stations between 24 and 26°E on the Agulhas Bank (1.1, 5.1, 5.2, 6.1, 7.1, 8.1) (Fig. 3d).

Average SML $Si(OH)_4$ concentrations ranged from 0.6 to 5.1 µmol Si L^{-1} (average: 3.0 ± 1.0 µmol Si L^{-1}) (Table S1) and showed only a moderate correlation with average SML NO_3 (Pearson's product moment, r = 0.40, p<0.005, n = 51). For the subtropical source waters of the Agulhas Bank, reported $Si(OH)_4$ concentrations are lower (<2 µmol Si L^{-1}) than many of the concentrations reported here, highlighting the importance of coastal upwelling (Lutjeharms et al., 1996), SML retention (through $bSiO_2$ dissolution; e.g. Brzezinski et al., 2003), and/or cross-thermocline fluxes of nutrients for the availability of Si in surface waters. The relative concentration of average SML $Si(OH)_4$ to NO_3, represented here by Si*, gave generally positive SML values (0 to 3.9) in surface waters (Fig. 3f), which differs to estimated Si* values (Si* 0 to -6, median Si* -3) based on the range of NO_3 and $Si(OH)_4$ concentrations reported for the subtropical source waters (see Lutjeharms et al., 1996). This contrast largely stems from the higher SML average $Si(OH)_4$ concentrations observed on the Bank during March 2019 (average: 3.0 ± 1.0 µmol Si L^{-1}) relative to the subtropical source waters (<2 µmol Si L^{-1}).

Interestingly, there was a noticeable trend of offshore stations having low or negative SML Si* values (0 to -1), with this pattern following the width of the shelf from east to west so that negative Si* values covered more of the shelf in the east than west (Fig. 3f). Low SML Si* values near the shelf edge are likely a proximate signal of the subtropical source waters for the Agulhas Bank, with their negative Si* values. Stations with negative Si* (indicating 'silicic acid depletion') had relatively high SML NO_3 concentrations (>2.6 µmol N

350 L^{-1}) indicating that it was not low $Si(OH)_4$ at these stations but rather high NO_3 that led to this pattern. This
351 pattern of negative Si* was not found at all stations with high NO_3 but was limited to stations on transects 2,
352 5, 6 and 7 (Fig. 3f). Strongly positive SML Si* values (>1) found more inshore and to the west of the sampling
353 grid on the Bank indicate 'nitrate-depletion' relative to $Si(OH)_4$ for diatoms on the Agulhas Bank in March or,
354 put another way, residual $Si(OH)_4$ in surface waters.
355
356 Bottom water average NO_3 concentrations in the BML ranged from 14.3 to 26.9 µmol N L^{-1} (average: 20.5 ±
357 2.9 µmol N L^{-1}) with low values (<18 µmol N L^{-1}) generally to the east around transect 1 (~27°E) and towards
358 the shelf break in the west (~22-23°E), while most stations had deep values between 18 and 22 µmol N L^{-1}
359 (Fig. 3d). Reported NO_3 concentrations for the South Indian Ocean Central Water (Fig. S2) that intrudes onto
360 the Bank are 8 to 18 µmol N L^{-1} (Lutjeharms et al., 1996), indicating that there must be NO_3 retention and/or
361 another source of NO_3 to bottom waters of the Bank (e.g. sedimentary nitrification). High BML average NO_3
362 concentrations (>22 µmol N L^{-1}) were limited to the offshore parts of the transects around 25°E (5 and 6) and
363 towards the inner shelf waters on the western section of the sampling grid (transects 11 and 12). Values of N*
364 for the BML were also negative (N* range -1.9 to -14.7, average N* -3.3 ± 2.0) (Fig. 3g), indicating depletion
365 of NO_3 relative to PO_4 in bottom waters of the Agulhas Bank. Estimates of N* for South Indian Ocean Central
366 Water, based on the nutrient values given by Lutjeharms et al. (1996), are also strongly negative (N* range -
367 4.8 to -14.0, median N* -9.4). The slight discrepancy of N* values between BML and South Indian Ocean
368 Central Water potentially also highlight a local source of NO_3 (independent of PO_4) to deep shelf waters (e.g.
369 sedimentary nitrification). An inshore-offshore pattern was observed with strongly negative N* values (less
370 than -4) inshore close to the coast and increasing N* values (-4 to -2) towards the shelf break (Fig. 3g). Strongly
371 negative N* values were also noticeable on the inner shelf to the west on transects 11 and 12. These patterns
372 in N* distribution potentially relate to a sedimentary source of NO_3 towards the inner Agulhas Bank, as
373 retention of remineralized organic matter would generate both N and PO_4 (and no pattern in N*).
374
375 In the case of BML Si*, there was a strong contrast to SML values, with Si* in the BML generally negative
376 (Si* range 2.4 to -8.5, average Si* -4.0 ± 2.6; Fig. 3h), indicative of 'silicic acid depletion' relative to NO_3 in
377 bottom waters. Negative Si* values are to be expected as South Indian Ocean Central Water is depleted in
378 $Si(OH)_4$ relative to NO_3 (Si* range -4.0 to -14.0, median Si* -9.0; estimated using values from Lutjeharms et
379 al., 1996), with the discrepancy between BML Si* and source water Si* again highlighting a potential local
380 (sedimentary) source of NO_3. Only 3 stations had positive Si* values in the BML (5.4, 5.5, 6.1), and these
381 were concentrated on the inshore-offshore transects near 25°E alongside negative values from -0.2 to -3; more
382 negative values (down to -8) were found offshore to the west of transects 5 and 6 while inshore waters had less
383 negative Si* values (Fig. 3h). As inshore BML waters had strongly negative N*, indicative of a local NO_3
384 source, positive Si* values are likely related to a proximate source of $Si(OH)_4$ that remains unidentified at this
385 time.
386
387 ***3.4. Phytoplankton biomass: Total and size-fractionated chlorophyll-a***

Surface concentrations of Chl*a*, from calibrated CTD fluorescence (FChl; see Methods), showed a patchy distribution across the Agulhas Bank in March (Fig. 4a). Values ranged from 0.3 mg m^{-3} to as high as 5.1 mg m^{-3} in surface waters across the sampling stations (average: 2.0 ± 1.1 mg m^{-3}), with high values (>3.1 mg m^{-3}) restricted to inshore waters around transect 7 and a few offshore stations near the shelf break. The range of these Chl*a* concentrations (FChl; 0.3-5.1 mg m^{-3}) agree with previous reviews and studies of the Agulhas Bank (Brown et al., 1991; Probyn et al., 1994; Barlow et al., 2010), including the observation of higher inshore and shelf break concentrations. No relationship was found between average SML NO_3 and SML FChl (Pearson product moment, $p = 0.11$, $n = 51$), highlighting that high surface Chl*a* occurred at both low (<1 µmol N L^{-1}) and high (>4 µmol N L^{-1}) NO_3 concentrations. This implies that different ecological dynamics were occurring in surface waters in autumn, ranging from 'post-bloom' (high Chl*a*, low nutrients) to 'pre-bloom' (low Chl*a*, high nutrients) or 'non-bloom' (low Chl*a*, low nutrients). Despite the trend of deepening of the SML from east to west (Fig. 2a), there was no similar trend in surface FChl (Fig. 4a).

Integrated full water column (i.e., surface to seabed) Chl*a* ($FChl_{0\text{-}bot}$), ranged from 22 to 196 mg m^{-2} (Fig. 4b; average: 69 ± 33 mg m^{-2}) and showed an east to west pattern. High values (>100 mg m^{-2}) were found inshore at the shallow station 1.1 (~27°E), towards the shelf break on transects 7 and 8 and were common at deep stations on transects 11 and 12 (Fig. 4b). In the east, high integrated water-column Chl*a* was associated with shallow water-columns (<60 m) whereas in the west high values were associated with deep water-columns (~200 m). A comparison of integrated Chl*a* over the euphotic zone ($FChl_{Eup}$) with water-column integrated Chl*a* ($FChl_{0\text{-}bot}$) showed that on average 85 ± 13% (range: 41-100%) of integrated Chl*a* was contained within the euphotic zone (i.e. shallower than the depth of penetration of 1% of incidental irradiance) (Fig. 4c). Stations with less than 70% of their total water column FChl in the euphotic zone were generally found on the most western sampling transects (11 and 12).

Across the eastern and central Agulhas Bank, 47% of stations possessed a definable SCM (i.e., sub-surface FChl greater than 1.5-times surface values; see Methods; Fig. 4d). Stations in the west with SCM corresponded to ones with less than 70% of total Chl*a* in the euphotic zone (Figs. 4c and 4d). According to our definition of a SCM, SCM on the Agulhas Bank varied in depth from 9 to 41 m (average: 22 ± 9 m), with generally shallow SCM (<20 m) east of ~23°E and deeper SCM to the west (>25 m; Fig. 4d). Peak FChl concentrations within the SCM ranged from 1.7 to 10.3 mg m^{-3} (average: 5.0 ± 2.7 mg m^{-3}) (Fig. 4e), with generally 2 to 33-times (average: 5 ± 7) more Chl*a* at depth in the SCM than in the overlying surface waters. Stations with SCM containing more than 10-times surface FChl values were restricted to transects 11 and 12 (stations: 11.1, 12.3, 12.5). Comparing SML and SCM depths (see Figs. 2a and 4d) shows that in general the SCM in autumn were at similar depths to the SML, with SCM in the east closer in depth to the SML than in the west. The percentage of surface irradiance (E_0) reaching the SCM (Fig. 4f), estimated using $K_{d(PAR)}$ and SCM depths, ranged from 0.4 to 31.8% (average: 8.7 ± 8.2%), with a strong east to west trend and SCM west of ~23°E generally receiving lower amounts of surface irradiance (0.4-6% of E_0).

Size-fractionated Chl*a* can be used as a simple indicator of the size-structure of the phytoplankton community, in our case giving the relative chlorophyll-biomass of picoplankton (0.2-2 µm), nanoplankton (2-20 µm) and microplankton (>20 µm). In surface waters across the Agulhas Bank in March, size-fractionated Chl*a* showed a patchy distribution of picoplankton relative biomass (as a percentage of total Chl*a*) (Fig. 5a), ranging from 2 to 80% (average: 29 ± 20%) with the highest contributions at one coastal (1.2) and two offshore stations (8.6 and 12.6). Nanoplankton relative chlorophyll-biomass ranged from 11 to 67% of total Chl*a* (average: 45 ± 20%), with most stations having 40 to 70% nanoplankton biomass (Fig. 5b). In contrast to picoplankton and nanoplankton relative chlorophyll-biomass, microplankton relative chlorophyll-biomass showed a noticeable east to west trend, with microplankton increasing in biomass in the west (Fig. 5c). Despite this east to west trend, microplankton only made up 4 to 45% (average: 26 ± 10%) of total chlorophyll-biomass, increasing from less than 20% in the east to 30 to 40% in the west.

3.5. Particulate organic carbon (POC), particulate nitrogen (PN), particulate silica ($bSiO_2$) and diatom cell abundance

Surface water concentrations of POC ranged from 86 to 570 mg C m^{-3} (average: 222 ± 106 mg C m^{-3}), with a slight east to west trend of stations with higher surface POC concentrations (>328 mg C m^{-3}) east of ~25°E and no clear or consistent inshore-offshore pattern (Fig. 6a). Surface PN concentrations ranged from 10 to 71 mg N m^{-3} (average: 32 ± 13 mg N m^{-3}; Table S1), showing a statistically significant relationship with surface POC concentrations (Pearson's product moment; r = 0.94, p<0.001, n = 29). Surface ratios of PN to POC (N:C) ranged from 0.10 to 0.17 mol mol^{-1} (average: 0.14 ± 0.02 mol mol^{-1}), indicating that in general particulate material had a similar ratio to the Redfield (1958) ratio of N to C (0.15 mol mol^{-1}), with values patchily distributed on the shelf (Fig. 6b). Comparison of surface Chl*a* (FChl) to POC concentrations, through the Chl:C ratio, showed that surface values ranged from 4 to 40 mg g^{-1} (average: 13 ± 8 mg g^{-1}), with no clear inshore-offshore or east to west pattern in the surface (Fig. 6c).

Surface water concentrations of $bSiO_2$ ranged from 0.10 to 4.51 µmol Si L^{-1} (average: 0.8 ± 0.9 µmol Si L^{-1}), with higher values (>2 µmol Si L^{-1}) limited to inshore stations on transects 2 (2.3) and 6 (6.1) and no clear pattern overall (Fig. 6d). Ratios of $bSiO_2$ to POC (Si:C; Fig. 6e) ranged from 0.01 to 0.18 mol mol^{-1} (average: 0.05 ± 0.05 mol mol^{-1}), with ratios higher than 0.13 mol mol^{-1} (the average diatom cellular Si:C ratio; Brzezinski, 1985) limited to stations 2.3, 6.1, 12.6 and 12.2. Diatom cell counts in surface waters (Fig. 6f) ranged from 520 to 12,000 cells L^{-1}, with the highest cell counts (>8,000 cells L^{-1}) limited to offshore stations rather than inshore stations on transects 8, 9, 10, 11 and 12. Whilst no statistically signification relationships existed between diatom cell numbers, POC and $bSiO_2$ (Pearson correlations, p > 0.1), there was a significant relationship of diatom abundance with >20 µm Chl*a* (r = 0.75, p<0.001, n = 25), indicating that ~56% of the variance in microplankton Chl*a* was related to diatom abundance.

3.6. Net Primary Production: Total and microplankton (>20 µm) NPP

At the six stations where daily rates of total net primary production (NPP) was measured for the euphotic zone (see Fig. 1), euphotic zone integrated NPP ranged from 0.3 to 1.1 g C m^{-2} d^{-1} (Table 1) with the highest integrated NPP found at station 8.6. Integrated measurements of microplankton (>20 µm) NPP showed 42 to 52% relative contributions apart from station 12.6, which had a microplankton contribution to NPP of 79% (Table 1). Microplankton contributions to total NPP were not the same as for their integrated contributions to total Chl*a*. Microplankton integrated Chl*a* ranged from 17 to 76% of total Chl*a* (Table 1), with station 12.6 having the highest contribution of microplankton to integrated Chl*a* (76%) and integrated NPP (79%). Generally, there was good agreement between euphotic zone integrated total Chl*a* and integrated total NPP, with stations with high NPP having high integrated Chl*a* (Table 1). However, the exception was station 1.1, which had the highest integrated Chl*a* (106 mg m^{-2}) of the stations where NPP was measured but the lowest integrated NPP (0.3 g C m^{-2} d^{-1}). Clearly, the phytoplankton dynamics at station 1.1 where quite distinct from that at other stations and are examined in more depth in the discussion (see section 4.3).

Plotting surface Chl*a* (FChl) against euphotic zone integrated NPP shows a strong positive linear relationship (Fig. 7) for most of the sampled stations (see Table 1), with the notable exception of station 1.1 which sits well removed from the linear relationship. The relationship between surface Chla (FChl) and integrated NPP can be described by a statistically significant (p<0.005) Modell II linear regression (Fig. 7). This regression can be used to estimate integrated NPP rates for sampling sites where NPP was not measured (Fig. 8), giving a total range of estimated integrated NPP in March of 0.1 to 1.1 g C m^{-2} d^{-1} (average: 0.4 ± 0.2 g C m^{-2} d^{-1}). Stations with high estimated NPP (>0.5 g C m^{-2} d^{-1}) were patchily distributed on the Agulhas Bank, though stations with low estimated NPP (<0.2 g C m^{-2} d^{-1}) where generally restricted to west of 25°E (Fig. 8).

4. Discussion

4.1. Net Primary Production on the Agulhas Bank

Measured NPP rates ranged from 0.3 to 1.1 g C m^{-2} d^{-1} for the six stations sampled (Table 1), with NPP based on surface calibrated fluorescence (FChl) concentrations ranging from 0.1 to 1.1 g C m^{-2} d^{-1} (average: 0.4 ± 0.2 g C m^{-2} d^{-1}; see Fig. 8) and showing a similar patchy distribution as FChl (Fig. 4a). Chlorophyll-normalized NPP (P^B; assimilation number), indicating production per unit chlorophyll-biomass, ranged from 0.3 to 1.5 g C (g Chl)$^{-1}$ h^{-1} (Table 1), implying relatively low-to-moderate productivity, for example the global average maximum value is 3.1 g C (g Chl)$^{-1}$ h^{-1} (Bouman et al., 2018). Assimilation numbers (P^B) vary with nutrient status and photo-acclimation, as well as temperature (Bouman et al., 2018), with the former factors likely important drivers of NPP on the Agulhas Bank (Carter et al., 1987; Probyn et al., 1994).

In-situ measurements of NPP on the Agulhas Bank have a sporadic spatial and temporal coverage, with studies often focusing on the upwelling cells in the east (e.g., Barlow et al., 2010; Lamont and Barlow, 2015) or the Benguela upwelling on the west coast (e.g., Brown et al., 1991; Barlow et al., 2009). By comparison, few studies have examined the central and eastern Agulhas Bank (20-27°E) (e.g. Carter et al., 1987; Probyn et al., 1994). Carter et al. (1987) reported primary production on the central and eastern Agulhas Bank, deploying short (<6 h) ^{14}C incubations to measure a range of 0.4 to 15 g C m^{-2} d^{-1} across five stations on the central Bank in March. High rates at one station (~15 g C m^{-2} d^{-1}) were associated with a SCM containing >40 mg m^{-3} of Chl*a*, while most stations had surface concentrations ~1 mg m^{-3} and SCM containing 2 to 6 mg m^{-3} (Carter et al., 1987), conditions more similar to the stations sampled in March 2019 (Fig. 4a, e). A review of primary productivity measurements by Probyn et al. (1994), also of short (<6 h) ^{14}C incubations, gave an area-weighted mean rate for the whole Agulhas Bank of 2 g C m^{-2} d^{-1} for summer. Taking the March measurements in Probyn et al. (1994), we estimate geometric means across the 95% confidence intervals reported of 1.7 g C m^{-2} d^{-1} (range: 0.1-14.7 g C m^{-2} d^{-1}) for the central Bank and 4.3 g C m^{-2} d^{-1} (range: 0.6 to 20.2 g C m^{-2} d^{-1}) for the eastern Bank. More recently, Barlow et al. (2010) measured primary production in spring on the central and eastern Agulhas Bank (22-29°E) ranging from 0.3 to 3.7 g C m^{-2} d^{-1}, with Lamont and Barlow (2015) further to the northeast on the KwaZulu-Natal shelf measuring rates of 0.4 to 9.9 g C m^{-2} d^{-1}.

Whilst there is some degree of overlap between our NPP measurements in March 2019 and those reported previously, especially at the lower end of the ranges, the highest NPP observed in our study was only 1.1 g C m^{-2} d^{-1} (Table 1). While we did not sample the chlorophyll rich SCM seen in several previous studies (Carter et al., 1987; Barlow et al., 2010), which could explain our lower NPP range, another important difference between studies were the techniques used (e.g. short-term versus 24 hr incubations, ^{14}C versus ^{13}C). Methodological differences can cause important differences, for example, our daily incubations would have measured NPP whereas shorter incubations (e.g. <6 h) scaled to daylength are more representative of gross primary production (Cullen, 2001). Satellite based measurements of NPP on the Agulhas Bank give average values for March of ~1 g C m^{-2} d^{-1} (Demarcq et al., 2008) and 1.2 to 1.9 g C m^{-2} d^{-1} (Mazwane et al., this issue), which are higher than this study (0.1-1.1 g C m^{-2} d^{-1}; average: 0.4 ± 0.2 g C m^{-2} d^{-1}).

Mazwane et al. (this issue) suggest that the Agulhas Bank ecosystem is more productive on an annual basis than other mid-latitude shelf sea systems (see also Probyn et al., 1994; Lutjeharms, 2007). Comparing our autumn measurements with similar in-situ measurements from mid-latitude systems shows similar NPP rates; for example, Poulton et al. (2019b) found NPP rates of 0.2 to 0.6 g C m^{-2} d^{-1} during autumn in the Celtic Sea (Northwest European Shelf), with similar rates during summer and higher rates during the spring bloom (0.7-6.4 g C m^{-2} d^{-1}; average: 2.4 ± 1.9 g C m^{-2} d^{-1}). The Agulhas Bank appears to lack a distinctive spring bloom of such intense productivity, though NPP remains relatively high and similar throughout the year (Demarcq et al., 2008; Mazwane et al., this issue), implying that continuously moderate NPP on the Agulhas Bank supports sustained production of the ecosystem. High NPP (>5 g C m^{-2} d^{-1}) appears more related to inshore upwelling zones along the South African coast than during seasonal bloom events (Mazwane et al., this issue), and

appears to have been missed by our sampling in March 2019. In contrast, compared to the neighboring Benguela upwelling, the Agulhas Bank has a lower productivity, for example Barlow et al. (2009) measured in-situ rates in the Benguela upwelling during late summer (February - March) of 0.4 to 8.2 g C m^{-2} d^{-1}.

Barlow et al. (2009) also highlighted variable relationships between in-situ measurements of Chl*a* and NPP, with stronger relationships in summer than winter in the Benguela upwelling. In our study we were restricted by the shortness of the autumn cruise in allowing only 7 daily measurements of NPP and while our relationship between surface FChl and NPP was statistically significant (p<0.001), this omitted one sampling station (1.1, ~27°E). Ideally, more sampling stations (e.g. >20) would lead to a more confident estimate of NPP from FChl. Station 1.1 had high FChl (2.9 mg m^{-3}) and low NPP (0.3 g C m^{-2} d^{-1}), with the chlorophyll-based NPP_{est} twice as high as that measured (0.6 g C m^{-2} d^{-1}). This discrepancy may relate to a previous high productivity (upwelling) event which had depleted surface NO_3 (<0.2 µmol N L^{-1}) (see Giering et al., this issue, for further discussion), and highlights how the dynamic oceanography of the eastern Agulhas Bank impacts productivity on short timescales.

In the future, more NPP measurements, alongside the kind of ancillary data collected here (e.g. size-fractionated Chl*a*, nutrients), and potentially using higher resolution techniques (e.g. fast-repetition-rate-fluorometry; Barlow et al., 2010) are needed to fully understand the spatial and temporal variability of the productivity of the central and eastern Agulhas Bank. Such NPP measurements would need to be collected following a standard protocol to allow for comparison between similar measurements and to account for important differences between techniques (Cullen, 2001). A level of confidence in our limited dataset can be found by the general agreement of our in-situ measurements with historical data (Carter et al., 1987; Probyn et al., 1994) and satellite-based estimates (Demarcq et al., 2008; Mazwane et al., this issue); however, we appeared to have missed the more elevated NPP often associated with coastal waters and intensive SCM on the Agulhas Bank.

4.2. What controls primary production on the Agulhas Bank in March?

4.2.1 Light availability: Light is a major driver of photosynthetic rates, with a strong decline in light with increasing depth. In autumn on the Agulhas Bank, despite euphotic zones varying by ~40 m (from 18 to 62 m; Fig. 3a), none of the sampled stations had SML depths greater than the euphotic zone and hence phytoplankton in the SML across the Bank always experienced more than 1% of incident irradiance. This contrasts with Barlow et al. (2010) in spring on the Agulhas Bank, where SML depths were 10 to 30 m deeper than euphotic zones. Estimates of the average irradiance a particle would encounter within the mixed layer ($\bar{E}_{SML}$) ranged from 26 to 76% (average: 44 ± 12%), with a decline in these values from east to west (Fig. 3b). Given an average of ~40 mol photons m^{-2} d^{-1} of incidental irradiance during March (see Mazwane et al., this issue), this range in $\bar{E}_{SML}$ equates to 10 to 30 mol photons m^{-2} d^{-1} (average: 18 ± 5 mol photons m^{-2} d^{-1}) of PAR. Estimates of the compensation irradiance, where photosynthetic rates equate to respiratory losses, range from 1.2 to 3.0

mol photons m^{-2} d^{-1} (Siegel et al., 2002; Venables and Moore, 2010; Wihsgott et al., 2019), which are ~10 times lower than the irradiance levels experienced by phytoplankton in the SML in March. These estimates of $\bar{E}_{SML}$ compare well with similar estimates in summer on the Patagonian Shelf (6-41 mol photons m^{-2} d^{-1}; Poulton et al., 2013) or in the Celtic Sea in spring and summer (10-18 and 9-20 mol photons m^{-2} d^{-1}, respectively), while autumn is much lower (<1 to 6 mol photons m^{-2} d^{-1}) (Poulton et al., 2019a, 2019b). Shallower SML than euphotic zone depths and considerable levels of SML irradiance indicate that light limitation was not an important factor limiting NPP in the SML during autumn on the Agulhas Bank, in contrast to other shelf seas.

While SML irradiance conditions were relatively high, around half of the stations sampled had a SCM which ranged in depth from east to west from ~10 to 40 m (Fig. 4d). The amount of surface irradiance reaching the SCM was only ~9% on average (range: 0.4-32%; Fig. 4f), lower than that experienced in the SML, with SCM in the west experiencing less than 6%. Previous work on the Agulhas Bank have found SCM, often with high rates of NPP, at the 3 to 7% surface irradiance depth (Carter et al., 1987), which is similar to our observations. Based on an incidental irradiance of ~40 mol photons m^{-2} d^{-1} (Mazwane et al., this issue), these equate to an average of ~3.6 mol photons m^{-2} d^{-1} (range: 0.2-13 mol photons m^{-2} d^{-1}), a value close to estimates of the compensation irradiance (1.2 to 3.0 mol photons m^{-2} d^{-1}; Siegel et al., 2002; Venables and Moore, 2010; Wihsgott et al., 2019) and indicating potential light limitation of the SCM. Irradiance data from March 2019 (GlobColour project; https://hermes.acri.fr/merged) averaged ~42 mol photons m^{-2} d^{-1} (range: 16-47 mol photons m^{-2} d^{-1}) which agrees well with the climatology of Mazwane et al. (this issue). While light limitation is not likely to influence NPP in the SML, it becomes more important when considering NPP in the SCM of the Agulhas Bank. Previously, Carter et al. (1987) found SCM at ~1% surface irradiance in summer on the central Agulhas Bank and concluded that the SCM on the bank were exclusively light limited.

4.2.2 Nutrient availability: As with the open ocean (Moore et al., 2013), nitrate appears to be a major limiting factor for NPP on the Agulhas Bank in autumn with the relative abundance of nitrate to phosphate showing depletion in nitrate relative to the Redfield (1958) ratio of 16:1, as shown by the negative N* values in surface waters across the Bank (Fig. 3e). Persistent negative N* values across the Bank contrast with the high surface NO_3 concentrations (>4-6.2 µmol N L^{-1}) found at several sampling sites offshore along transects 5, 6 and 7 (Fig. 3c). Such high surface nutrient levels are surprising, with the expectation that phytoplankton would rapidly deplete such levels and thus some additional process may be involved. Examination of the maximum buoyancy frequency values (N^2) across the Agulhas Bank (Fig. 2d) show that stations on transects 5, 6 and 7 had low N^2 values (<2 $x10^3$ s^{-1}), implying that weaker stratification at these stations relates to the elevated surface NO_3.

Negative N* values indicate nitrate depletion relative to phosphate, but do not necessarily confirm proximate nitrate limitation of surface NPP. Rather, the availability of NO_3 relative to the N requirements to support NPP (i.e. 'N-demand') gives an idea of whether NO_3 is sufficient to support the observed rates of NPP. The N-

demand to support NPP can be estimated by converting NPP rates into N units, and here we use the N:C ratio (0.13 mol mol^{-1}) from nutrient-replete phytoplankton (Geider and La Roche, 2002) to convert NPP. Due to the unknown contribution of detrital and/or bacterial biomass to the bulk POC values measured, a phytoplankton-specific N:C is more appropriate than the value for particulate material on the Bank (0.14 mol mol^{-1}) or the global average from Redfield (1958) (0.15 mol mol^{-1}).

Plotting N-demand against average SML NO_3 concentrations shows most stations (n = 45) fall below the 1:1 unity line (Fig. 9) with SML NO_3 sufficient to support instantaneous rates of measured and estimated NPP; however, there are several exceptions (n = 12) where surface NO_3 appears insufficient to support NPP. These stations include inshore stations to the east (1.1, 5.2, 7.1) and west (12.1, CR4) and offshore stations in the middle (8.3, 8.4, 8.5, 8.6) of the sampling grid. To support NPP rates at these stations, alternative nitrogenous compounds (ammonium, urea) are required, although differences between N-demand and SML NO_3 at these stations are often <0.2 µmol N L^{-1} (Fig. 9). Even if N-demand were to be doubled (e.g., higher rates of NPP, higher N:C ratios), many stations would still have NO_3 concentrations >1 µmol N L^{-1} above the estimated N-demand. For example, if the Redfield (1958) N:C ratio (0.15 mol mol^{-1}) was used to estimate N-demand, there is no change in the number of stations which are considered to have sufficient NO_3 to support NPP (n = 45; see Fig. S3).

That only 21% of stations required additional sources of N, whereas SML NO_3 concentrations were able to support NPP rates at the other 79%, is a surprising observation and implies that sufficient NO_3 was found in the SML at most stations on the Agulhas Bank in autumn. Moreover, calculating the turnover time of SML average NO_3 based on our estimates of N-demand gives an average of ~11 ± 12 days (range: 1-60 days), implying that surface phytoplankton communities have sufficient NO_3 to support continued rates of NPP for around another week before they are dependent on alternative sources (e.g. coastal and shelf-edge upwelling, vertical fluxes through the thermocline). During our autumn survey of the Bank, we did not observe strong upwelling of deep waters, with strong stratification maintained at many of the inshore sites associated with upwelling cells (Fig. 2d). The pycnocline in autumn was characterized by high values (>4 x 10^{-3} s^{-2}) of buoyancy frequency (Fig. 2d) and steep gradients in temperature (1-2°C m^{-1}; Largier and Stewart, 1987; Swart and Largier, 1987; Carter et al.,1987; Lutjeharms, 2006). Such a strong thermocline will regulate vertical fluxes of nutrients such as nitrate (Probyn et al., 1994; Sharples et al., 2001), with bottom waters replenished with nutrients from the South Indian Central Water advected onto the shelf (Fig. S2; Lutjeharms et al., 1996; Jackson et al., 2012). While SML NO_3 concentrations appear sufficient to continue to fuel NPP for short periods, away from the coastal upwelling sites, vertical diffusive fluxes of nutrients regulated by the stability of the thermocline will be key to maintaining NPP. There is thus a need to understand the mixing and thermocline phytoplankton dynamics (e.g., Sharples et al., 2001) of the Agulhas Bank to address seasonal production.

Sufficient NO_3 to support rates of NPP for many stations across the Agulhas Bank in autumn implies a reliance on NO_3 for much of the NPP, and hence high '*f*-ratios' (sensu Dugdale and Goering, 1967). These simple estimates indicate a lack of proximate nitrate limitation of primary production on the Agulhas Bank in autumn and highlight the potential for an abundance of organic matter for higher trophic levels (or export to depth) during this time. Particulate N:C ratios on the bank at the time of sampling (average: 0.14 ± 0.02 mol mol^{-1}; see Fig. 6b) were between both the Redfield ratio (0.15 mol mol^{-1}; Redfield, 1958) and that of nutrient replete phytoplankton (0.13 mol mol^{-1}; Geider and La Roche, 2002), showing only moderate enrichment in C (min. 0.12 mol mol^{-1}), implying that the particulate material formed was relatively N-rich, further supporting a lack of direct NO_3 limitation and a high *f*-ratio; both of which would have decreased particulate N:C ratios.

Whilst the availability of nitrogen (and phosphorus) controls the distribution and activity of the entire phytoplankton community, silicic acid is a key limiting nutrient for diatoms, which tend to characterize more productive coastal ecosystems (Tréguer and De La Rocha, 2013). On the Agulhas Bank in March, $Si(OH)_4$ concentrations were generally higher than the notional 2 µmol Si L^{-1} concentration believed to limit diatom productivity (Egge and Aksnes, 1992), with most surface waters having positive Si* values higher than 2 (Fig. 3g) and indicative of residual silicic acid concentrations (Bibby and Moore, 2011). There was also an inshore to offshore trend in the SML Si* values, with offshore values becoming lower and, in some cases, negative (especially transects 5, 6 and 7), a clear signal of the low $Si(OH)_4$ concentrations (<2 µmol Si L^{-1}) of the subtropical source waters (see Results 3.3). Whilst this pattern of offshore negative Si* did not correspond to particulate silica ($bSiO_2$) distribution (Fig. 6d), it was noticeable that diatom abundances in surface waters were higher offshore near the shelf break than they were inshore (Fig. 6f). Elevated diatom abundance near the shelf break likely relate to localized upwelling and frontal interactions with the Agulhas Current (Boyd and Shillington, 1994; Probyn et al., 1994; Jackson et al., 2012; Lutjeharms, 2006; Malan et al., 2018).

4.2.3 Mortality: Whilst a few studies have examined meso-zooplankton (>200 µm) biomass on the Agulhas Bank (Verheye et al., 1994; Peterson and Hutchings, 1995; Noyon et al., this issue), none have measured grazing rates or the potential of zooplankton to have a strong grazing impact on phytoplankton communities. During March 2019, Noyon et al. (this issue) measured secondary production by meso-zooplankton at the same CTD stations sampled in this study, with a comparison of secondary production ('zooplankton C-demand') and our estimated NPP showing that 29% of the stations sampled had zooplankton C-demand exceeding NPP, while around half of stations had C-demand ~50% of estimated NPP. The results of Noyon et al. (this issue) imply that meso-zooplankton exert a strong control on rates of NPP across the Agulhas Bank in autumn and support our conclusions about abundant organic material for higher trophic levels and a potentially high *f*-ratio characterizing the phytoplankton communities on the Bank. Hutchings (1994), Verheye et al. (1994) and Peterson and Hutchings (1995) estimate that Agulhas Bank zooplankton could consume approximately 20 to 60% of NPP, with dense copepod concentrations exerting a strong grazing control on NPP and being strongly correlated to Chl*a* concentrations (including the SCM).

To summarize, the SML of the Agulhas Bank in autumn appears to have ample irradiance and nitrate to support observed and estimated rates of daily NPP, with only a few stations (18%) requiring alternative nitrogenous sources (ammonium, urea). Nitrate-depletion relative to phosphate (negative N*) are characteristic of Bank waters, and likely inherited from the subtropical source water for the SML (see Results 3.3). Support for NPP from NO_3 on the Agulhas Bank in autumn implies that 'new production' (sensu Dugdale and Goering, 1967) characterizes production on the Bank (Carter et al., 1987), with relatively N-rich particulate material supporting the idea that recycling is of limited importance during autumn. Moreover, N-rich particulate material and NPP supporting estimates of zooplankton production (Noyon et al., this issue) indicate that the Agulhas Bank in autumn is a productive system for both primary and secondary producers. Residual silicic acid concentrations were common on the Agulhas Bank at the time of sampling, indicating other factors (e.g. selective grazing, competition for nitrate) limited diatom production on the Bank.

4.3. Does the Subsurface Chlorophyll Maximum contribute to production?

Around half of the stations sampled on the Agulhas Bank in March possessed a clearly definable SCM (Fig. 4d) where Chl*a* concentrations at depth where more than 1.5-times higher than in surface waters. It is thus a reasonable question to ask whether these SCM also represented deep productivity maximum, as seen for SCM in other shelf seas (e.g. Holligan et al., 1984a, b; Hickman et al., 2012) and previously observed on the Agulhas Bank (Carter et al., 1987; Probyn et al., 1994; Barlow et al., 2010). The clear east to west trend of deepening SCM (Fig. 4d), associated with a decline in SCM irradiance levels (Fig. 4f), also implies that different processes may be important in the formation and maintenance of the SCM (Cullen, 1982, 2015). Relatively high absolute irradiances at the SCM allow elevated nitrate uptake (new production) relative to light limited SCM (Cullen, 1982, 2015; Carter et al., 1987; Hickman et al., 2012), although the absolute irradiance experienced relative to the vertical gradient in nitrate is a key determinant (Cullen, 2015). While the SCM deepened across the Bank, vertical gradients in nitrate (0.9-1.4 µmol NO_3 L^{-1} m^{-1}) and the density of the nitracline (24.9-26.1 kg m^{-3}) were similar (Table 2).

SCM may form by in-situ growth and productivity, sinking of surface biomass onto a density discontinuity, photo-adaptation of phytoplankton deep in the water column in association with deep nutrient pools, or some combination of these (Cullen, 1982, 2015; Carter et al., 1987). Deep measurements of NPP were only made at six sites across the Agulhas Bank, and of these only three had SCM present (Table 2); two inshore sites to the east (1.1, 5.1) and one inshore site in the west (CR4). At these three sites, and indeed for all the stations sampled for NPP, surface rates of NPP were similar (range: 25.1-37.2 mg C m^{-3} d^{-1}), while SCM NPP rates were different between eastern (1.6-8.1 mg C m^{-3} d^{-1}) and western (0.4 mg C m^{-3} d^{-1}) stations. Deep NPP rates, where measured, were 3- to 16-times lower than surface rates in the east, and 80-times lower in the west, whereas the assimilation number (P^B) lacked such east to west differences; P^B ranged from 0.1 to 0.3 g C (g FChl)$^{-1}$ h^{-1} in the east and from <0.1 to 0.2 g C (g FChl)$^{-1}$ h^{-1} in the west (Table 2). These are lower than the values reported by Carter et al. (1987) on the Agulhas Bank in summer when SCM were strong productivity maxima (0.6-2.9

g C (g Chl)$^{-1}$ h^{-1}) or by Barlow et al. (2010) in spring (>5 g C (g Chl)$^{-1}$ h^{-1}), and indicate that the SCM sampled in March 2019 were associated with low rates of production per unit (chlorophyll) biomass.

For the SCM on the Agulhas Bank to represent a deep NPP maximum, or equal surface NPP (average: 35 ± 15 mg C m^{-3} d^{-1}; Table 2), it would need to have equivalent P^B to surface waters and contain ~13 mg Chl*a* m^{-3} or if depth-dependent patterns of P^B remained it would need to contain at least 145 mg m^{-3} of Chl*a*. Thus, for SCM to represent deep NPP maxima they require both high P^B and relatively high Chl*a* concentrations (>10 mg m^{-3}; see Holligan et al., 1984a, b; Carter et al., 1987; Barlow et al., 2010) – a pattern not seen in autumn but observed by other Agulhas Bank studies. Two stations on the western Agulhas Bank in March 2019 possessed SCM with Chl*a* concentrations ~10 mg m^{-3} (Stations 12.5, CR4; Fig. 4e) but both had low relative light levels in the SCM (~0.4%), potentially highlighting the role of light limitation in deep productivity in the west. Carter et al. (1987) observed SCM containing 5 to 10 mg m^{-3} during summer on the central Agulhas Bank (20-23°E) while Barlow et al. (2010) observed SCM of 2 to 5 mg m^{-3} around the eastern Agulhas Bank in spring. Both Carter et al. (1987) and Barlow et al. (2010) identified the SCM as making important contributions to integrated productivity (see also Probyn et al., 1994), linking SCM productivity to deep photo-physiology, although photosynthetic rates remained higher in surface waters.

While the SCM have FChl concentrations over 1.5-times higher than surface values (roughly 2-times higher for the eastern sites and 5-times higher in the west), surface and deep POC concentrations were similar (Table 2). This implies that the SCM Chl:C ratio was different than in surface waters, and indeed the SCM Chl:C (FChl:POC) ratio in the east was 6 to 13 mg g^{-1}, which is similar to the range generally seen in surface waters (5-12 mg g^{-1}; Fig. 6c), while in the SCM in the west it was roughly doubled (~17-22 mg g^{-1}). A previous estimate of SCM Chl:C ratios for the Agulhas Bank found an average ratio of ~15 (± 5) mg g^{-1} (Carter et al., 1987). Changes in Chl:C ratios indicate photo-acclimation as cellular levels of pigmentation increase to enhance light harvesting at low light (Geider et al., 1998; Cullen, 2015). As Chl:C ratios are similar to surface values in the SCM in the east (Table 2, Fig. 6c), photo-acclimation may play a minor role in formation of the SCM there, whereas the 2-times higher Chl:C ratios in the SCM in the west relative to surface values (Table 1) implies photo-acclimation is important in the formation of the SCM in the west. Declining irradiance in the SCM from east to west (Fig. 4f: average east of 25°E, 16 ± 9%; average west of 25°E, 6 ± 6%) confirm an increasing importance of light harvesting against a trend of declining light availability.

For most stations sampled across the Agulhas Bank, SML average NO_3 concentrations appear sufficient to support surface NPP rates (Fig. 9), with notable exceptions in inshore waters. In the case of the SCM (Table 2), NO_3 concentrations are similar, or slightly higher, in the east and 90-times higher than surface values in the west. Gradients of NO_3 and average density associated with the nitracline are similar between sites in the east and west (Table 2). Comparing N-demand to support deep NPP rates, in a similar way as with surface waters (see Fig. 9), shows that the SCM in both the east and west have sufficient NO_3 to support SCM NPP (Table 2); the SCM is not nutrient limited, but appears differentially light-limited east and west.

765

766 SCM are important sites for 'new production' and nitrate-uptake due to proximity to high nitrate fluxes
767 (Dugdale and Goering, 1967; Holligan et al., 1984b; Carter et al., 1987; Sharples et al., 2001; Letelier et al.,
768 2004; Hickman et al., 2012; Cullen, 2015), and this appears true of the SCM on the Agulhas Bank, which are
769 found with relatively high NO_3 concentrations and NO_3 gradients (1-9 µmol N L^{-1} and 0.9-1.4 µmol N L^{-1} m^{-1}
770 ; Table 2). Beyond the concentration of nitrate at the SCM, the flux of nutrients into the SCM and SML is
771 another key determinant of the processes involved in SCM formation and its role in new production (Dugdale
772 and Goering, 1967; Holligan et al., 1984b; Carter et al., 1987; Sharples et al., 2001; Hickman et al., 2012;
773 Cullen, 2015); shallow SCM in the east may receive higher fluxes of nitrate, and support higher new
774 production, whereas deep SCM in the west may be rate limited by the flux of nitrate and the strong thermoclines
775 occurring there (Fig. 2d).
776
777 For March 2019, a paradox exists between 'sufficient' NO_3 to support NPP in the SML and the presence of
778 SCM. How can a SCM associated with N-uptake co-occur with high surface NO_3 concentrations? Reexamining
779 the stations with SCM, median SML NO_3 concentrations were ~0.3 µmol N L^{-1} (range: 0.1-4.8 µmol N L^{-1}),
780 with only four stations with NO_3 over 1 µmol N L^{-1} (5.1, 5.5, 9.2, 12.5), and median NPP rates for stations
781 with SCM were ~0.2 g C m^{-2} d^{-1}. Generally, stations with SCM were associated with low SML NO_3 and low
782 NPP, although there were exceptions. The presence of a SCM despite elevated SML NO_3 highlights dynamic
783 processes within the thermocline. For example, cross-thermocline fluxes of 1 to 3 mmol N m^{-2} d^{-1} have been
784 estimated in the Celtic Sea (Sharples et al., 2001), which over a 20 to 30 m SML equate to 0.03 to 0.15 µmol
785 N L^{-1} d^{-1} if the SCM was unable to utilize this flux. With SML NO_3 of ~0.3 µmol N L^{-1}, such fluxes could
786 replenish SML NO_3 in only 2 to 10 days (assuming no uptake in the SCM or SML).
787
788 Light availability in the SCM controls N-uptake (Letelier et al., 2004; Hickman et al., 2012; Cullen, 2015) so
789 that variability in irradiance could lead to slightly elevated SML NO_3. While average incidental irradiance in
790 March 2019 was ~42 ± 7 mol photons m^{-2} d^{-1} (range: 16-47 mol photons m^{-2} d^{-1}; GlobColour project), at times
791 it dropped to <20 mol photons m^{-2} d^{-1}, which in the SCM would equate to only ~1.8 mol photons m^{-2} d^{-2}, based
792 on the SCM receiving an average of ~9% of surface irradiance. This average value is close to estimates of the
793 compensation irradiance (1.2-3.0 mol photons m^{-2} d^{-1}; Siegel et al., 2002; Venables and Moore, 2010; Wihsgott
794 et al., 2019) indicating that the SCM could become severely light limited on occasion, allowing NO_3 to
795 accumulate in the SML. Conversely, when irradiance reaches 47 mol photons m^{-2} d^{-1} this would equate to ~3.7
796 mol photons m^{-2} d^{-1}, which highlights that the SCM on the Agulhas Bank may at times also have high light
797 availability, strengthening N-uptake and NPP.
798
799 Based on limited observations from March on the Agulhas Bank, where sampled, the SCM was not a
800 productivity maximum but varied from east to west in terms of whether it was a maximum in phytoplankton
801 biomass or pigment, respectively. Moderate NPP and irradiance, and low Chl:C, imply that the eastern SCM
802 are biomass maxima associated with elevated productivity, although maximum NPP remained in surface

waters (Table 2). Low (<1 mg C m^{-3} d^{-1}) NPP rates, high Chl:C and low irradiance imply that the SCM in the west is a pigment maximum, formed through photo-acclimation, with maximum NPP occurred in surface waters (Table 2). Of the stations sampled, only 47% had SCM, while the rest had uniform or only slight increases in Chl*a* concentrations in the SML. Of those where a SCM was present, we only sampled three for NPP and hence there is a need to sample a far wider number of SCM across the Agulhas Bank to fully examine east to west gradients in SCM formation, maintenance, and productivity. However, based on the east to west gradients in SML depth (Fig. 2a), buoyancy frequency (Fig. 2d), NO_3 concentration (Fig. 3c) and SCM irradiance (E_{SCM}; Fig. 4f), it appears reasonable to assume that the longitudinal trends in our small number of stations reflects the larger-scale pattern. Without higher levels of deep biomass and irradiance, it appears unlikely that the SCM on the Agulhas Bank in autumn represent deep productivity maxima, though they may remain important contributors to integrated NPP and new production.

4.4. Phytoplankton community composition

Across the Agulhas Bank in autumn, nanoplankton (2-20 µm) dominated total Chl*a* (average: 45% ± 20%), with picoplankton (0.2-2 µm) slightly more abundant than microplankton (>20 µm) (averages: 29% ± 20% and 26% ± 10%, respectively). Despite the low relative contribution to total Chl*a*, microplankton were the only phytoplankton size class to show a clear east to west trend of increasing contributions (Fig. 5c). Phytoplankton size-structure has important implications for pelagic ecosystem dynamics, with microplankton (diatoms, dinoflagellates) important for the transfer of material to higher trophic levels (zooplankton, fish larvae). Despite low relative and absolute levels of microplankton Chl*a* (<30% and 0.06-0.66 mg m^{-3}, respectively), there was close coupling between primary production and zooplankton secondary production on the bank in autumn (Noyon et al., this issue). Hence, either zooplankton were reliant on nanoplankton production (Huggett et al., 2000) or there was an efficient trophic transfer between small phytoplankton and zooplankton (Verheye et al., 1994; Calbet and Landry, 2004; Schmoker et al., 2013). Further, at the 6 stations where integrated NPP was measured (Table 1), microplankton contributions to NPP were relatively high (average: 51% ± 14%; range: 42-79%) and matched the zooplankton C demands (Noyon et al., this issue). Clearly, further measurements are needed to explore these patterns during the productive late summer and autumn periods.

Particulate silica ($bSiO_2$), an indicator of siliceous diatom biomass, was low (<1 µmol Si L^{-1}) across the Agulhas Bank (Fig. 6d) with particulate Si:C ratios lower (Fig. 6e) than average diatom Si:C ratios (0.13 mol mol^{-1}; Brzezinski, 1985). Low Si:C ratios and low contributions of microplankton Chl*a* to total Chl*a* (<30%) indicate that most of the particulate material was not associated with diatom cells, though there were a couple of notable exceptions with ratios greater than 0.13 mol mol^{-1} (stations 2.3, 7.1, 12.2, 12.6) where diatoms may have contributed more to the particulate pool (Fig. 6e). Diatom cell counts showed little relationship with $bSiO_2$ or Si:C ratios, with highest diatom cell counts towards the shelf break rather than inshore (Fig. 6f). However, there was a statistically significant relationship between microplankton Chl*a* and diatom cell counts (r = 0.75, p>0.001, n = 25), indicating that diatoms were related to ~56% of the spatial variability in

841 microplankton Chl*a* and there were higher diatom contributions to the west. A lack of a similar pattern in
842 $bSiO_2$ and Si:C ratios implies that diatoms on the Agulhas Bank had more variable Si:C ratios than the average
843 diatom ratio (0.13 mol mol^{-1}; Brzezinski, 1985) and may have been lightly silicified. Diatom taxa such as
844 *Chaetoceros* and *Pseudonitzschia* have Si:C ratios ~0.03 to 0.05 mol mol^{-1} (Brzezinski, 1985), much closer to
845 the ratios measured on the Agulhas Bank in autumn (<0.06 mol mol^{-1}; Fig. 6e). In fact, light microscope
846 observations of diatoms across the Agulhas Bank during our study were dominated by genera such as
847 *Pseudonitzschia* and *Navicula*.
848
849 **5. Conclusions**
850
851 Our measurements and estimates of NPP on the Agulhas Bank in March 2019 ranged from 0.1 to 1.1 g C m^{-2}
852 d^{-1}, which were in reasonable agreement with historical in-situ and satellite measurements during summer and
853 autumn. While stations with high Chl*a* and NPP were patchily distributed on the Agulhas Bank, there was a
854 trend for western stations to have lower Chl*a* and NPP. SCM were detected at around half of the sampling
855 stations, though no extremely chlorophyll-rich SCM (>10 mg m^{-3}) were observed, with these features
856 historically being associated with deep productivity maximum and/or as significant contributors to integrated
857 NPP on the Agulhas Bank.
858
859 Surface mixed layers on the Agulhas Bank had sufficient light for photosynthesis during March, with daily
860 irradiance conditions in the SML more similar to spring and summer conditions in other temperate systems.
861 Nutrient conditions in the SML were estimated to be adequate to support observed rates of NPP, despite often
862 low NO_3 concentrations, although the strong thermocline characteristic of the Agulhas Bank may limit
863 diffusive nutrient fluxes and influence NPP dynamics over longer timescales and away from sites of coastal
864 and shelf edge upwelling.
865
866 The SCM of the Agulhas Bank are regarded as important contributions to NPP and N-cycling, though previous
867 studies have highlighted the potential for light-limitation of SCM productivity. Our survey in March 2019
868 observed a strong east to west gradient in the dynamics of the SCM, including the potential for light-limitation,
869 their role as sites of deep new production, and their contribution to integrated NPP. For the SCM sampled in
870 this study, the conditions for them to represent deep maxima of NPP appear not to have been met (e.g. high
871 chlorophyll-biomass >10 mg m^{-3}, high assimilation numbers), although we only examined a few SCM in detail
872 and thus there is clearly a need for fuller examination of SCM dynamics across the Agulhas Bank in autumn
873 (and summer) to elucidate their role in ecosystem productivity and nutrient cycling. Moreover, due to the
874 potentially limiting nature of the strong thermocline on the bank for nutrient fluxes, dynamic processes (e.g.
875 mixing due to internal tides, reduced irradiance due to cloudy days) need to be examined further to understand
876 the control(s) on NPP in autumn.
877

While nanoplankton appear to dominate biomass across the Agulhas Bank in autumn, microplankton were present, and, while only representing a third of chlorophyll-biomass, they often represented over 50% of NPP. A strong correlation between diatoms cell counts and variability of the microplankton Chl*a* fraction indicate that diatoms are important contributors to microplankton biomass. Examination of particulate Si:C ratios indicate that lightly silicified diatoms (e.g., *Chaetoceros*, *Pseudonitzschia*, *Navicula*) are present on the Agulhas Bank, which is surprising as there were significant levels of residual $Si(OH)_4$ in the SML across the bank. Such residual $Si(OH)_4$ contrasts strongly with the silica-depleted nature (negative Si*) of the subtropical surface water for the SML (Si* -3) and the deeper South Indian Ocean Central Water (Si* -4) which is advected into the bottom waters of the Bank. Indeed, the sources and cycling processes of Si in the waters of the Agulhas Bank are another interesting future research question due to the importance of diatoms in supporting secondary production.

Author contributions

Alex J Poulton: Funding acquisition, Conceptualization, Investigation, Formal analysis, Writing – original draft, Writing – review and editing; **Sixolile L Mazwane:** Conceptualization, Investigation, Formal analysis, Writing – review and editing; **Brian Godfrey:** Data curation, Investigation, Formal analysis, Writing – review and editing; **Filipa Carvalho:** Data curation, Investigation, Formal analysis, Writing – review and editing; **Juliane Wihsgott:** Data curation, Investigation, Formal analysis, Writing – review and editing; **Edward Mawji:** Data curation, Investigation, Formal analysis, Writing – review and editing; **Margaux Noyon:** Conceptualization, Investigation, Formal analysis, Writing – original draft, Writing – review and editing.

Acknowledgements

We thank the captain and crew of the RV *Ellen Khuzwayo*, as well as the Department of Agriculture, Forestry and Fisheries (now DFFE). We are also thankful to the scientists of the SOLSTICE-WIO project for fruitful discussions. This publication was produced with the financial support of the Global Challenges Research Fund (GCRF), UK, in the framework of the SOLSTICE-WIO project, NE/P021050/1. This work was supported by the UK-SA Bilateral Chair of Ocean Science and Marine Food Security funded by the NRF/DST Grant (98399) and Newton Funds.

References

Barlow, R., Lamont, T., Mitchell-Innes, B., Lucas, M., Thomalla, S., 2009. Primary production in the Benguela ecosystem, 1999-2002. Afr. J. Mar. Sci. 31, 97-101. https://doi.org/10.2989/AKMS.2009.31.1.9.780.

Barlow, R., Lamont, T., Kyewalyanga, M., Sessions, H., Morris, T., 2010. Phytoplankton production and physiological adaptation on the south-eastern shelf of the Agulhas ecosystem. Cont. Shelf. Res. 30, 1472-1486. https://doi.org/10.1016/j.csr.2010.05.007.

Bauer, J.E., Cai, W-J., Raymond, P.A., Bianchi, T.S., Hopkinson, C.S., Regnier, P.A.G., 2013. The changing carbon cycle of the coastal ocean. Nature 504, 61-70. https://doi.org/10.38/nature12857.

Becker, S., Aoyama, M., Woodward, E.M.S., Bakker, K., Coverly, S., Mahaffey, C., Tanhua, T., 2020. GO-SHIP repeat hydrography nutrient manual: The precise and accurate determination of dissolved inorganic nutrients in seawater, using continuous flow analysis methods. Front. Mar. Sci. 7, 581790. https://doi.org/10.3389/fmars.2020.581790.

Bibby, T.S., Moore, C.M., 2011. Silicate:nitrate ratios of upwelled waters control the phytoplankton community sustained by mesoscale eddies in sub-tropical North Atlantic and Pacific. Biogeosci. 8, 657-666. https://doi.org/10.5194/bg-8-657-2011.

Bouman, H.A., Platt, T., Doblin, M., Figueiras, F.G., Gudmundsson, J., Gudfinnsson, H.G., Huang, B., Hickman, A., Hiscock, M., Jackson, T., Lutz, V.A., Melin, F., Rey, F., Pepin, P., Segura, V., Tilstone, G.H., van Dongen-Volels, V., Sathyendranath, S., 2018. Photosynthesis-irradiance parameters of marine phytoplankton: synthesis of a global data set. Earth Syst. Sci. Data 10, 251-266. https://doi.org/10.5194/essd-10-251-2018.

Boyd, A.J., Taunton-Clark, J., Oberholster, G.P.J., 1992. Spatial features of the near-surface and midwater circulation patterns off western and southern South Africa and their role in the life histories of various commercially fished species. S. Afr. J. Mar. Sci. 12, 189-206. https://doi.org/10.2989/02577619209504702.

Boyd, A.J., Shillington, F.A., 1994. Physical forcing and circulation patterns on the Agulhas Bank. South Afr. J. Sci. 90, 143–154. https://doi.org/10.10520/AJA00382353_4624.

Brown, P.C., Painting, S.J., Cochrane, K.L., 1991. Estimates of phytoplankton and bacterial biomass and production in the northern and southern Benguela ecosystems. S. Afr. J. Mar. Sci. 11, 537-564. https://doi.org/10.2989/025776191784287673.

Brzezinski, M.A., 1985. The Si:C:N ratio of marine diatoms: interspecific variability and the effect of some environmental variables. J. Phycol. 21, 347-357. https://doi.org/10.1111/j.0022-3646.198.00347.x

Brzezinski, M.A., Jones, J.L., Bidle, K.D., Azam, F., 2003. The balance between silica production and silica dissolution in the sea: Insights from Monterey Bay, California, applies to the global data set. Limnol. Oceanogr. 48, 1846-1854. https://doi.org/10.4319/lo.2003.48.5.1846.

Calbet, A., Landry, M.R., 2004. Phytoplankton growth, microzooplankton grazing, and carbon cycling in marine ecosystems. Limnol. Oceanogr. 49, 51-57. https://doi.org/10.4319/lo.2004.49.1.0051.

Carter, R.A., McMurray, H.F., Largier, J.L., 1987. Thermocline characteristics and phytoplankton dynamics in Agulhas Bank waters. S. Afr. J. Mar. Sci. 5, 327-336. https://doi.org/10.2989/025776187784522306.

Carvalho, F., Kohut, J., Oliver, M.J., Schofield, O., 2017. Defining the ecologically relevant mixed-layer depth for Antarctica's coastal seas. Geophys. Res. Lett. 44, 338–345. https://doi.org/10.1002/2016GL071205.

Chapman, P., Largier, J., 1989. On the origin of the Agulhas Bank bottom water. S. Afr. J. Sci. 85, 515-519.

Cullen, J.J., 1982. The deep chlorophyll maximum: comparing vertical profiles of chlorophyll *a*. Can. J. Fish. Aqu. Sci. 39, 791-803. https://doi.org/10.1139/f82-108.

Cullen, J.J., 2001. Primary production methods. In: Encyclopedia of Ocean Sciences (Eds. Steele, J., Thorpe, S., Turekian, K), Academic Press, London, pp. 2277-2284. https://doi.org/10.1006/rwos.2001.0203.

954 Cullen, J.J., 2015. Subsurface chlorophyll maximum layers: Enduring enigma or mystery solved? Ann. Rev.
955 Mar. Sci. 7, 207-239. https://doi.org/101146/annurev-marine-010213-135111.
956 Daniels, C.J., Poulton, A.J., Esposito, M., Paulsen, M.L., Bellerby, R., St John, M., Martin, A.P., 2015.
957 Phytoplankton dynamics in contrasting early-stage North Atlantic spring blooms: composition,
958 succession, and potential drivers. Biogeosci. 12, 2395-2409. https://doi.org/10.5194/bg-12-2395-2015.
959 Demarcq, H., Barlow, R., Shillington, F.A., 2003. Climatology and variability of sea surface temperature and
960 surface chlorophyll in the Benguela and Agulhas regions as observed by satellite imagery. Afr. J. Mar.
961 Sci. 25, 363-372. https://doi.org/10.2989/18142320309504022.
962 Demarcq, H., Richardson, A.J., Field, J.G., 2008. Generalised model of primary production in the southern
963 Benguela upwelling system. Mar. Ecol. Prog. Ser. 354, 59-74. https://doi.org/10.3354/meps07136.
964 Dugdale, R.C., Goering, J.J., 1967. Uptake of new and regenerated forms of nitrogen in primary
965 productivity. Limnol. Oceanogr. 12, 196-206. https://doi.org/10.4319/lo.1967.12.2.0196.s.
966 Egge, J.K., Aksnes, D.L., 1992. Silicate as regulating nutrient in phytoplankton competition. Mar. Ecol.
967 Prog. Ser. 83, 281-289. https://doi.org/10.3354/meps083281.
968 Field, C.B., Behrenfeld, M.J., Randerson, J.T., Falkowski, P., 1998. Primary production of the biosphere:
969 Integrating terrestrial and oceanic components. Science 281, 237-240.
970 https://doi.org/10.1126/science.281.5374.237.
971 Gieder, R., MacIntyre, H.L., Kana, T., 1998. A dynamic regulatory model of phytoplanktonic acclimation to
972 light, nutrients, and temperature. Limnol. Oceanogr. 43, 679-694.
973 https://doi.org/10.4319/lo.1998.43.4.0679.
974 Geider, R., La Roche, J., 2002. Redfield revisited: variability of C:N:P in marine microalgae and its
975 biochemical basis. Eur. J. Phycol. 37, 1-17. https://doi.org/10.1017/S0967026201003456.
976 Giering, S.L.C., Noyon, M., Godfrey, B., Poulton, A.J., Carvalho, F., Roberts, M. This Issue. Optical particle
977 measurements indicate resuspension as dominant mechanism behind the formation of benthic nepheloid
978 layers on the Agulhas Bank. Deep-Sea Res. II,
979 Goschen, W.S., Schumann, E.H., Bernard, K.S., Bailey, S.E., Deyzel, S.H.P., 2012. Upwelling and ocean
980 structures off Algoa Bay and the south-east coast of South Africa. Afr. J. Mar. Sci. 34,525-536.
981 http://dx.doi.org/10.2989/1814232X.2012.749810.
982 Hickman, A.E., Moore, C.M., Sharples, J., Lucas, M.I., Tilstone, G.H., Krivtsov, V., Holligan, P.M., 2012.
983 Primary production and nitrate uptake within the seasonal thermocline of a stratified shelf sea. Mar. Ecol.
984 Prog. Ser. 463, 39-57. https://doi.org/10.3354/meps09836.
985 Holligan, P.M., Williams, P.J.L., Purdie, D., Harris, R.P., 1984a. Photosynthesis, respiration, and nitrogen
986 supply of plankton populations in stratified, frontal and tidally mixed shelf waters. Mar. Ecol. Prog. Ser.
987 17, 201-213. https://doi.org/10.3354/MEPS017201.
988 Holligan, P.M., Harris, R.P., Newell, R.C., Harbour, D.S., Head, R.N., Linley, E.A.S., Lucas, M.I., Tranter,
989 P.R.G., Weekley, C.M., 1984b. Vertical distribution and partitioning of organic carbon in mixed, frontal,
990 and stratified waters of the English Channel. Mar. Ecol. Prog. Ser. 14, 111-127.
991 https://doi.org/10.3354/MEPS014111.

Hopkins, J.E., Palmer, M.R., Poulton, A.J., Hickman, A.E., Sharples, J., 2021. Control of a phytoplankton bloom by wind-driven vertical mixing and light availability. Limnol. Oceanogr. 66, 1926-1949. https://doi.org/10.1002/lno.11734.

Huggett, J.A., Richardson, A.J., 2000. A review of the biology and ecology of *Calanus agulhensis* off South Africa. ICES J. Mar Sci. 57, 1834-1849. https://doi.org/10.1006/jmsc.2000.0977.

Hutchings, L., 1994. The Agulhas Bank: a synthesis of available information and a brief comparison with other east-coast shelf regions. S. Afr. J. Sci. 90, 179-185. https://hdl/handle.net/10520/AJA00382353_4628.

Hutchings, L., Beckley, L.E., Griffiths, M.H., Roberts, M.J., Sundby, S., van der Lingen, C., 2002. Spawning on the edge: Spawning grounds and nursery areas around the southern African coastline. Mar. Fresh. Res. 53, 307–318. https://doi.org/10.1071/MF01147.

Hutchinson, K., Beal, L.M., Penven, P., Ansorge, I., Hermes, J., 2018. Seasonal phasing of Agulhas Current transport tied to a baroclinic adjustment of near-field winds. J. Geophys. Res. Oceans 123, 7067-7083. https://doi.org/10.1029/2018JC014319.

Jackson, J.M., Rainville, L., Roberts, M.J., McQuaid, C.D., Lutjeharms, J.R.E., 2012. Mesoscale bio-physical interactions between the Agulhas Current and the Agulhas Bank, South Africa. Cont. Shelf Res. 49, 10–24. https://doi.org/10.1016/j.csr.2012.09.005.

Kirk, J.T.O., 1983. Light and photosynthesis in aquatic ecosystems. Cambridge University Press, Cambridge, 401 pp.

Lamont, T., Barlow, R.G., 2015. Environmental influence of phytoplankton production during summer on the KwaZulu-Natal shelf of the Agulhas ecosystem. Afr. J. Mar. Sci. 37, 485-501. https://doi.org/10.2989/1814232X.2015.1108228.

Lamont, T., Brewin, R.J.W., Barlow, R.G., 2018. Seasonal variation in remotely-sensed phytoplankton size structure around southern Africa. Rem. Sens. Env. 204, 617-631. https://doi.org/10.1016/j.rse.2017.09.038.

Largier, J.L., Swart, V.P., 1987. East-west variation in thermocline breakdown on the Agulhas Bank. S. Afr. J. Mar. Sci. 5, 263-272. https://doi.org/10.2989/025776187784522252.

Legendre, L., Gosselin, M., 1996. Estimation of N and C uptake rates by phytoplankton using ^{15}N and ^{13}C: revisiting the usual computation formulae. J. Plankt. Res. 19, 263-271. https://doi.org/10.1093/plankt/19.2.263.

Letelier, R.M., Karl, D.M., Abbott, M.R., Bidigare, R.R., 2004. Light driven seasonal patterns of chlorophyll and nitrate in the lower euphotic zone of the North Pacific Subtropical Gyre. Limnol. Oceanogr. 49, 508-519. https://doi.org/10.4319/lo.2004.49.2.0508.

Longhurst, A., Sathyendranath, S., Platt, T., Caverhill, C., 1995. An estimate of global primary production in the ocean from satellite radiometer data. J. Plank. Res. 17, 1245-1271. https://doi.org/10.1093/plankt/17.6.1245.

Lutjeharms, J.R.E., 2006. The Agulhas Current. Springer-Verlag, Berlin Heidelberg. https://doi.org/10.1007/3-540-37212-1.

Lutjeharms, J.R.E., 2007. Three decades of research on the greater Agulhas Current. Ocean Sci. 3, 12—147. https://doi.org/10.5194/os-3-129-2007.

Lutjeharms, J.R.E., Meyer, A.A., Ansorge, I.J., Eagle, G.A., Orren, M.J.,1996. The nutrient characteristics of the Agulhas Bank. S. Afr. J. Mar. Sci. 17, 253-274.

Malan, N., Backeberg, B., Biastoch, A., Durgadoo, J.V., Samuelsen, A., Reason, C., Hermes, J., 2018. Agulhas Current Meanders Facilitate Shelf-Slope Exchange on the Eastern Agulhas Bank. J. Geophys. Res. Oceans 123, 4762–4778. https://doi.org/10.1029/2017JC013602.

Mazwane, S.L., Poulton, A.J., Hickman, A.E., Jebri, F., Jacobs, Z., Roberts, M., Noyon, M. This Issue. Seasonal and long-term stability of Net Primary Production on the Agulhas Bank, 1998-2018. Deep-Sea Res. II

Moore, C.M., Mills, M.M., Achterberg, E.P., Geider, R.J., LaRoche, J., Lucas, M.I., McDonagh, E.L., Pan, X., Poulton, A.J., Rijkenberg, M.J.A., Suggett, D.J., Ussher, S.J., Woodward, E.M.S., 2009. Large-scale distribution of Atlantic nitrogen fixation controlled by iron availability. Nature Geo. 2, 867-871. https://doi.org.10.1038/ngeo667.

Moore, C.M., Mills., M.M., Arrigo, K.R., Berman-Frank, I., Bopp, L., Boyd, P.W., Galbraith, E.D., Geider, R.J., Guieu, C., Jaccard, S.L., Jickells, T.D., La Roche J., Lenton, T.M., Mahowald, N.M., Marañón, E., Marinov, I., Moore, J.K., Nakatsuka, X., Oschlies, A., Saito, M.A., Thingstand, T.F., Tsuda, A., Ulloa, O., 2013. Processes and patterns of oceanic nutrient limitation. Nature Geo. 6, 701-710. https://doi.org/10.1038/ngeo1765.

Noyon, M., 2019. Ellen Khuzwayo EK188 – Cruise Summary Report. Southampton. pp. 61. https://www.bodc.ac.uk/resources/inventories/cruise_inventory/reports/ellenkhuzwayo_188.pdf.

Noyon, M., Poulton, A.J., Asdar, S., Weitz, R., Giering, S.L. This Issue. Zooplankton community structure on the Agulhas Bank in autumn: size structure and growth. Deep-Sea Res. II

Painter, S.C., Finlay, M., Hemsley, V.S., Martin, A.P., 2016. Seasonality, phytoplankton succession and the biogeochemical impacts of an autumn storm in the northeast Atlantic Ocean. Prog. Oceanogr. 142, 72-104. https://doi.org/10.1016/j.pocean.2016.02.001.

Pauly, D., Christensen, V., Guenette, S., Pitcher, T.J., Sumaila, R., Walters, C.J., Watson, R., Zeller, D., 2002. Towards sustainability in world fisheries. Nature 418, 689-695. https://doi.org.10.1038/nature01017.

Peterson, W.T., Hutchings, L., 1995. Distribution, abundance, and production of the copepod *Calanus agulhensis* on the Agulhas Bank in relation to spatial variations in hydrography and chlorophyll concentration. J. Plank. Res. 17, 2275-2294. https://doi.org/10.1093/plankt/17.12.2275.

Poulton, A.J., Young, J.R., Bates, N.R., Balch, W.M., 2011. Biometry of detached *Emiliania huxleyi* coccoliths along the Patagonian Shelf. Mar. Ecol. Prog. Ser. 443, 1-17, https://doi.org/10.3354/meps09445.

Poulton, A.J., Painter, S.C., Young, J.R., Bates, N.R., Bowler, B., Drapeau, D., Lyczsckowski, E., Balch, W.M., 2013. The 2008 *Emiliania huxleyi* bloom along the Patagonian Shelf: Ecology, biogeochemistry, and cellular calcification. Global Biogeochem. Cycl. 27, 1-11. https://doi.org/10.1002/2013GB004641.

1068 Poulton, A.J., Mayers, K.M.J., Daniels, C.J., Stinchcombe, M.C., Woodward, E.M.S., Hopkins, J., Wihsgott,
1069 J.U., Widdicombe, C.E., 2019a. Dissolution dominates silica cycling in a shelf sea autumn bloom.
1070 Geophys. Res. Lett. 46, 6765-6774. https://doi.org/10.1029/2019GL083558
1071 Poulton, A.J., Davis, C.E., Daniels, C.J., Mayers, K.M.J., Harris, C., Tarran, G.A., Widdicombe, C.E.,
1072 Woodward, E.M.S., 2019b. Seasonal phosphorus and carbon dynamics in a temperate shelf sea (Celtic
1073 Sea). Prog. Oceanogr. 177, 101872. https://doi.org/10.1016/j.pocean.2017.11.001.
1074 Probyn, T.A., Mitchellinnes, B.A., Brown, P.C., Hutchings, L., Carter, R.A., 1994. A review of primary
1075 production and related processes on the Agulhas Bank. South Africa. J. Sci. 90, 166-173.
1076 https://hdl.handle.net/10204/2018.
1077 Ragueneau, O., Tréguer, P., 1994. Determination of biogenic silica in coastal waters: applicability and limits
1078 of the alkaline digestion method. Mar. Chem. 45, 43-51. https://doi.org/10.1016/0304-4203(94)90090-6.
1079 Redfield, A.C, 1958. The biological control of chemical factors in the environment. Am. Sci. 46, 205-221.
1080 https://www.jstor.org/stable/27827150.
1081 Schmoker, C., Hernandez-Leon, S., Calbet, A., 2013. Microzooplankton grazing in the oceans: impacts, data
1082 availability, knowledge gaps and future directions. J. Plankt. Res. 35, 691-706.
1083 https://doi.org/10.1093/plankt/fbt023.
1084 Schumann, E.H., Perrins, L.A., Hunter, I.T., 1982. Upwelling along the south coast of the Cape Province,
1085 South Africa. S. Afr. J. Sci. 78, 238-242.
1086 Siegel, D.A., Doney, S.C., Yoder, J.A., 2002. The North Atlantic spring phytoplankton bloom and
1087 Sverdrup's critical depth hypothesis. Science 296,730-733. https://doi.org/10.1126/science.1069174.
1088 Sharples, J. Moore, C.M., Rippeth, T.P., Holligan, P.M., Hydes, D.J., Fisher, N.R., Simpson, J.J., 2001.
1089 Phytoplankton distribution and survival in the thermocline. Limnol. Oceanogr. 46, 486-496.
1090 https://doi.org/10.4319/lo.2001.46.3.0486.
1091 Swart, V.P., Largier, J.L., 1987. Thermal structure of Agulhas Bank water. S. Afri. J. Mar. Sci. 5, 243–252.
1092 https://doi.org/10.2989/025776187784522153.
1093 Tréguer, P., De La Rocha, C.L., 2013. The world ocean silica cycle. Ann. Rev. Mar. Sci. 5, 477-501.
1094 https://doi.org/10.1146/annurev-marine-121211-172346.
1095 Venables, H., Moore, C.M., 2010. Phytoplankton and light limitation in the Southern Ocean: Learning from
1096 high-nutrient, high-chlorophyll areas. J. Geophys. Res. Atm. 115. https://doi.org/10.1029/2009JC005361.
1097 Verheye, H.M., Hutchings, L., Huggett, J.A., Carter, R.A., Peterson, W.T., Painting, S.J., 1994. Community
1098 structure, distribution, and trophic ecology of zooplankton on the Agulhas Bank with special reference to
1099 copepods. S. Afr. J. Sci. 90, 154-165. https://journals.co.za/doi/pdf/10.10520/AJA00382353_4635.
1100 Welschmeyer, N.A., 1994. Fluorometric analysis of chlorophyll-*a* in the presence of chlorophyll-*b* and
1101 phaeopigments. Limnol. Oceanogr. 39, 1985-1992. https://doi.org/10.4319/lo.1994.39.8.1985.
1102 Wihsgott, J.U., Sharples, J., Hopkins, K.E., Woodward, E.M.S., Hull, T., Greenwood, N., Sivyer, D.B.,
1103 2019. Observations of vertical mixing in autumn and its effect on the autumn phytoplankton bloom. Prog.
1104 Oceanogr. 177, 102059. https://doi.org/10.1016/j.pocean.2019.01.001.

TABLES

Table 1. Hydrography and euphotic zone integrals for phytoplankton biomass and composition, net primary production, particulate material, and stoichiometric ratios.

Table 2. Surface mixed layer (SML) and subsurface chlorophyll maximum (SCM) characteristics in terms of phytoplankton biomass and composition, net primary production, particulate material, stoichiometric ratios, and nitrate and light availability. For stations for which no SCM was present (8.6, 9.1b, 10.2, and 12.6) in-situ sampling concentrated on the base of the SML and NPP incubations were at the 4.5% surface irradiance level (see Methods).

FIGURES

Fig. 1. Sampling stations along inshore-offshore transects from east to west on the Agulhas Bank (March 2019) superimposed on a satellite composition (6/3/19-22/4/19) of surface Chla concentration (4-km MODIS Aqua data). The diversity of sampling at each station is indicated in the key, with transects numerated east to west and from inshore (low digits) to offshore (high digits). Bathymetry contours (black lines) for 200 m and 100 m are provided.

Fig. 2. Hydrological characteristics of the sampling stations: (a) Surface Mixed Layer (SML) depth (m); (b) Seasurface temperature (ºC); (c) Depth of the buoyancy frequency maximum (N^2, m); (d) Maximum buoyancy frequency (N^2, x 10^{-3} s^{-2}); (e) Bottom Mixed Layer (BML) depth (m); and (f) BML thickness (m). Panel (a) indicates the numbering from east to west of the inshore-offshore sampling transects.

Fig. 3. Light and macronutrient regimes: (a) Depth of the euphotic zone (Z_{Eup}, m); (b) SML average irradiance ($\bar{E}_{SML}$, % of surface irradiance, E_0); (c) SML average NO_3 (µmol N L^{-1}); (d) BML average NO_3 (µmol N L^{-1}); (e) SML average N*; (f) SML average Si*; (g) BML average N*; and (h) BML average Si*. Panel (a) indicates the numbering from east to west of the inshore-offshore sampling transects.

Fig. 4. Chlorophyll-a distribution and Subsurface Chlorophyll Maximum (SCM): (a) Surface calibrated-fluorescence (FChl, mg m^{-3}); (b) Water-column integrated $FChl_{0\text{-}bot}$ (mg m^{-2}); (c) Fraction of $FChl_{Eup}$ / $FChl_{0\text{-}bot}$; (d) Depth of the SCM (Z_{SCM}, m); (e) SCM FChl (mg m^{-3}); and (f) Irradiance at the depth of SCM (E_{SCM}) as a percentage of surface irradiance (E_0). Empty circles in d-f indicate that no SCM was present (see Methods). Panel (a) indicates the numbering from east to west of the inshore-offshore sampling transects.

Fig. 5. Size-fractionated Chl*a* as a percentage (%) of total chlorophyll-*a* in surface waters; (a) Picoplankton (0.2-2 µm) Chl*a*; (b) Nanoplankton (2-20 µm) Chl*a*; and (c) Microplankton (>20 µm) Chl*a*. Empty circles indicate no measurements. Panel (a) indicates the numbering from east to west of the inshore-offshore sampling transects.

Fig. 6. Particulate material and diatoms in surface waters; (a) Particulate organic carbon (POC, mg C m^{-3}); (b) Particulate nitrogen to carbon ratio (N:C, mol:mol); (c) Chl*a* to carbon ratio (mg:g); (d) Particulate silica ($bSiO_2$, mmol Si L^{-1}), (e) Particulate silica to carbon ratio (Si:C, mol:mol); and (f) Surface diatom cell abundances (cells L^{-1}). Empty circles indicate no measurements. Panel (a) indicates the numbering from east to west of the inshore-offshore sampling transects.

Fig. 7. Scatter plot between surface Chl*a* (FChl; mg m^{-3}) and euphotic zone integrated NPP (g C m^{-2} d^{-1}). Individual stations are identified, and Model II Linear regression presented.

Fig. 8. Estimated Net Primary Production (g C m^{-2} d^{-1}) from surface Chl*a* measurements. Inshore-offshore sampling transects are labelled and numerated from east to west.

Fig. 9. Comparison of surface NO_3 concentrations (µmol N L^{-1}) with estimates of N-demand (µmol N $L^{-1}d^{-1}$) based on using Geider and La Roche's (2002) nutrient-replete phytoplankton N:C ratio (0.13 mol mol^{-1}) to convert surface rates of NPP. Note log-log scale with dashed line indicating 1:1 ratio. Open circles represent estimates from sampled stations (Table 1) while grey circles are NPP estimates from surface Chl*a* using the regression in Figure 7. Sampling sites above the 1:1 line indicate potential TON limitation of NPP rates, whereas sites below the dashed line are considered TON replete.

SUPPLEMENTARY TABLE

Table S1. Surface and deep physio-chemical data from the Agulhas Bank, including surface mixed layer (SML) silicic acid ($Si(OH)_4$), SML phosphate (PO_4), surface particulate nitrogen (PN), SML average salinities, bottom mixed layer (BML) average temperature, BML average salinity, BML phosphate (PO_4), and BML silicic acid ($Si(OH)_4$).

SUPPLEMENTARY FIGURES

Fig. S1. Scatter plot of Surface Mixed Layer depth (m) defined by a 0.125 kg m^{-3} difference between surface and deep values against the depth (m) of the maximum buoyancy frequency (N^2). Dashed line indicates unity. Pearson production moment correlation statistics are given.

Fig. S2. Temperature-Salinity diagram of CTD data from the Agulhas Bank in March 2019. Panel A) shows all profile data; and B) shows profile data from CTD casts along three inshore-offshore transects along the Agulhas Bank (see Fig. 1 for transect locations). Dominant water masses are indicated in terms temperature ranges as Agulhas Bank water masses have similar salinity ranges (after Jackson et al., 2012).

Fig. S3. Comparison of surface NO_3 concentrations (µmol N L^{-1}) with estimates of N-demand (µmol N L^{-1} d^{-1}) based on using the Redfield (1958) N:C ratio (0.15 mol mol^{-1}) to convert surface rates of NPP. Note log-log scale with dashed line indicating 1:1 ratio. Open circles represent estimates from sampled stations (Table 1) while grey circles are NPP estimates from surface Chl*a* using the regression in Figure 7. Sampling sites above the 1:1 line indicate potential NO_3 limitation of NPP rates, whereas sites below the dashed line are considered NO_3 replete.

Table 1.

Parameter	Sampling sites 1.1	5.1	8.6	10.2	12.6	CR4	Units
Latitude (ºS)	33º38’	34º00’	34º43’	34º28’	35º35’	34º52’	
Longitude (ºE)	26º54’	25º13’	23º43’	22º20’	22º06’	22º42’	
Chlorophyll-*a*	106	28	61	27	64	61	[mg m^{-2}]
Microplankton	63	34	47	17	76	47	[%]
Net Primary Production (NPP)	0.32	0.41	1.11	0.47	0.69	0.47	[g C m^{-2} d^{-1}]
Microplankton NPP	44	46	52	42	79	44	[%]
Assimilation number (P^B)	0.3	1.2	1.5	1.5	0.9	0.6	[g C (g Chl)$^{-1}$ h^{-1}]

Table 2.

Parameter	Sampling sites 1.1	5.1	8.6	9.1 b	10.2	12.6	CR4	Units
Surface Mixed Layer								
Chlorophyll-*a* (FChl)	2.9	1.0	2.9	0.9	1.3	3.3	2.0	[mg m^{-3}]
Net Primary Production (NPP)	25.0	26.3	68.7	30.5	26.8	37.2	32.2	[mg C m^{-3} d^{-1}]
Microplankton (>20 µm) NPP	26	48	54	37	50	68	59	[%]
Particulate silica ($bSiO_2$)	0.8	0.8	1.5	ND	0.3	1.2	ND	[µmol Si L^{-1}]
Chl-normalised NPP	0.7	2.2	2.0	2.8	1.7	0.9	1.3	[g C (g FChl)$^{-1}$ h^{-1}] [a]
Chl:C (FChl:POC)	5	4	12	ND	5	28	11	[mg g^{-1}]
Si:C ($bSiO_2$:POC)	0.02	0.03	0.07	ND	0.01	0.12	0.01	[mol:mol]
N:C (PN:POC)	0.12	0.17	0.15	ND	0.17	0.13	0.14	[mol:mol]
NO_3	0.2	1.2	0.1	0.8	0.5	0.5	0.1	[µmol N L^{-1}]
N-demand [b]	0.3	0.3	0.9	0.4	0.3	0.5	0.4	[µmol N L^{-1} d^{-1}]
NO_3/N-demand	0.7	3.5	0.1	2.0	1.5	1.0	0.3	[days]
Average SML irradiance ($\bar{E}_{SML}$)	56	63	53	45	48	31	29	[%]
Subsurface Chlorophyll Maximum or 4.5% Surface irradiance (E_0) incubations								
Depth of the CM (ZCM)	20	9	-	-	-	-	39	[m]
Sampling depth	21	8	10	18	14	16	26	[m]
Chlorophyll-*a* (FChl)	6.4	1.7	3.8	0.9	1.6	3.8	3.3	[mg m^{-3}]
Net Primary Production (NPP)	8.1	2.1	13.5	ND	3.2	7.7	0.4	[mg C m^{-3} d^{-1}]
Microplankton (>20 µm) NPP	79	25	19	ND	0	54	ND	[%]
Particulate silica ($bSiO_2$)	2.6	ND	1.2	ND	ND	ND	0.9	[µmol Si L^{-1}]
FChl-normalised NPP	0.1	0.1	0.3	ND	0.2	0.2	<0.1	[g C (g FChl)$^{-1}$ h^{-1}] [a]
Chl:C (FChl:POC)	13	6	14	4	8	22	17	[mg g^{-1}]
Si:C ($bSiO_2$:POC)	0.06	0.03	0.04	0.06	ND	ND	0.06	[mol:mol]
N:C (PN:POC)	0.14	0.17	0.19	0.17	0.18	0.16	0.16	[mol:mol]
NO_3	0.7	1.3	2.8	1.2	6.7	0.5	9.0	[µmol N L^{-1}]
NO_3 gradient [c]	1.3	1.4	0.9	1.4	1.2	1.2	1.4	[µmol NO_3 L^{-1} m^{-1}]
Density of NO_3-gradient [d]	26.1	25.5	25.8	25.8	25.4	24.9	25.6	[kg m^{-3}]
N-demand [b]	0.1	<0.1	0.2	ND	<0.1	0.1	<0.1	[µmol N L^{-1} d^{-1}]
NO_3/N-demand	7	49	16	ND	166	6	1772	[days]
Relative Irradiance (E_0)	4	31	20	21	16	7	0.3	[%]

[a] calculated assuming a 12-hour day; [b] calculated as NPP divided by 12 (to correct for moles) and then by 0.13 (average N:C ratio following Geider and La Roche (2002)); [c] NO_3-gradient calculated as maximum change in NO_3 concentration with depth; [d] median density over depth range where maximum NO_3-gradient observed.

Figure 1.

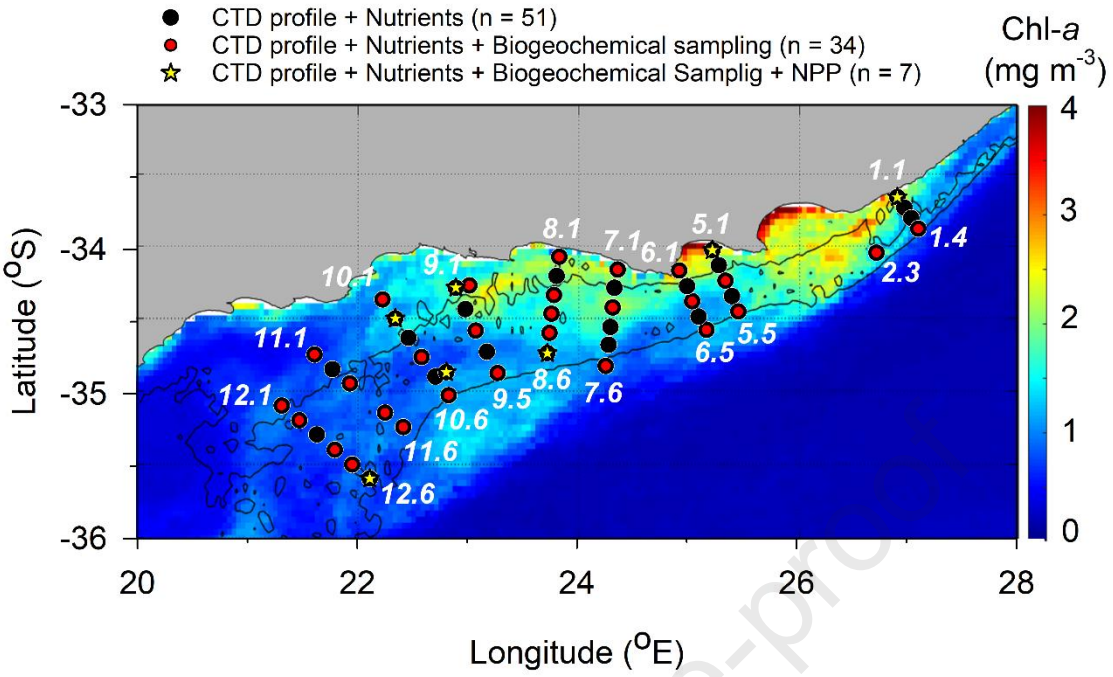

Figure 2.

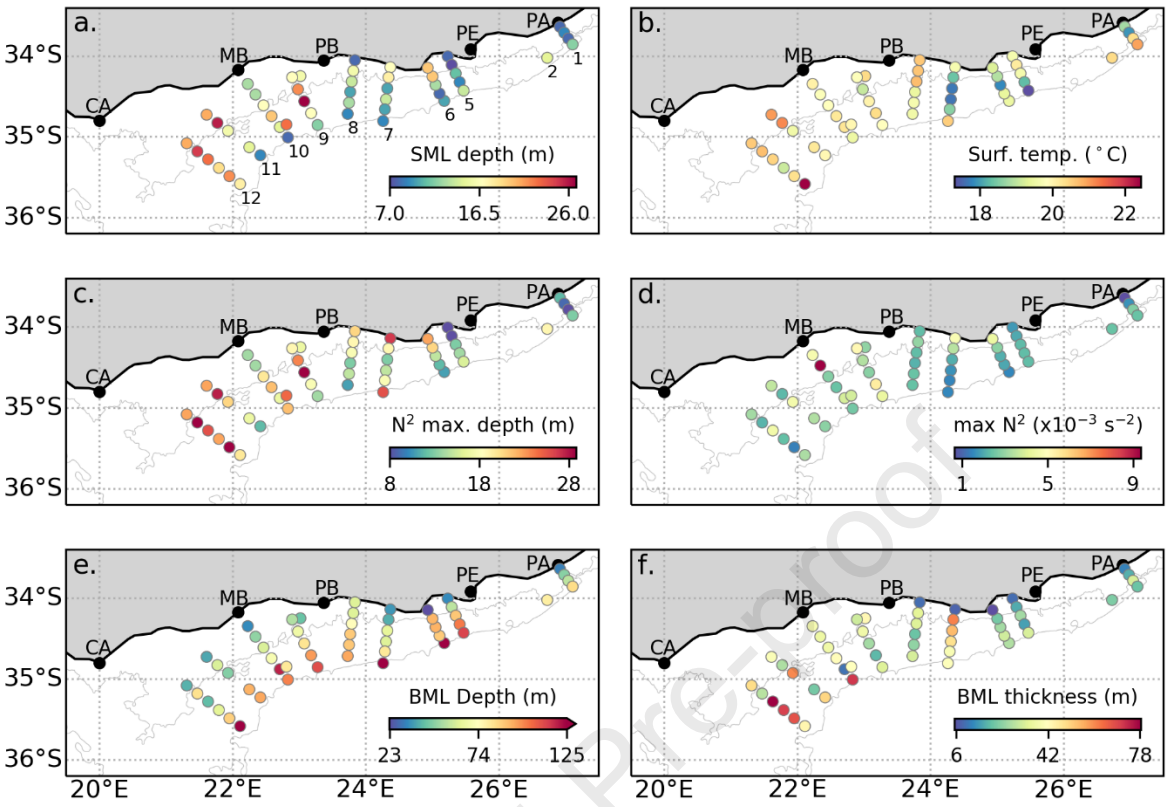

Figure 3.

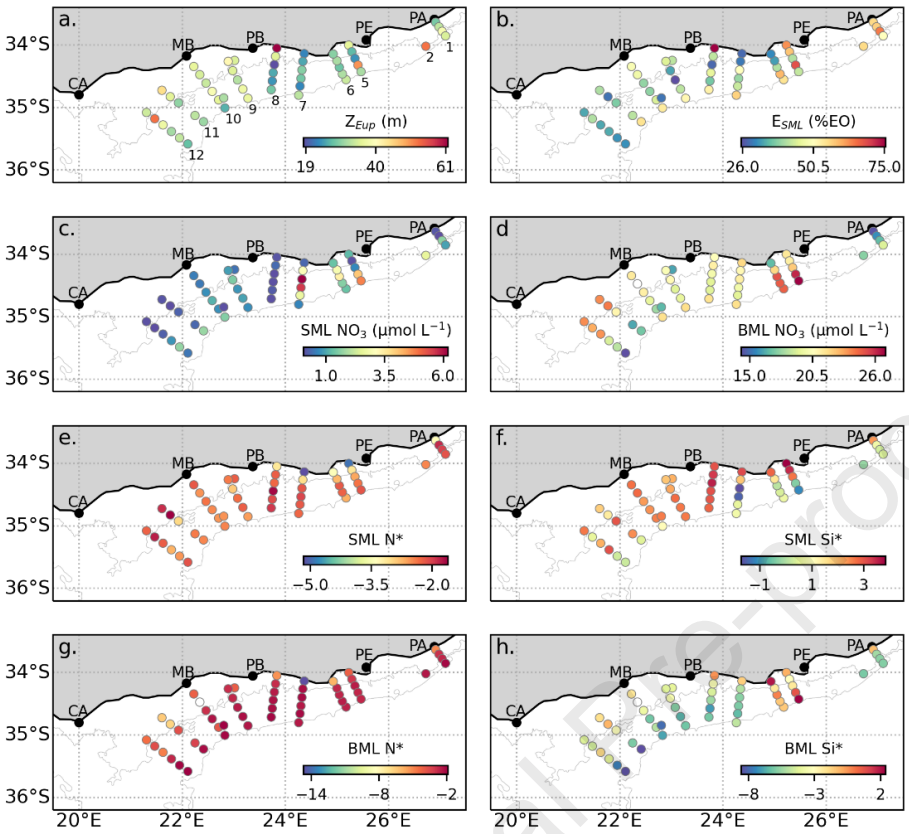

Figure 4.

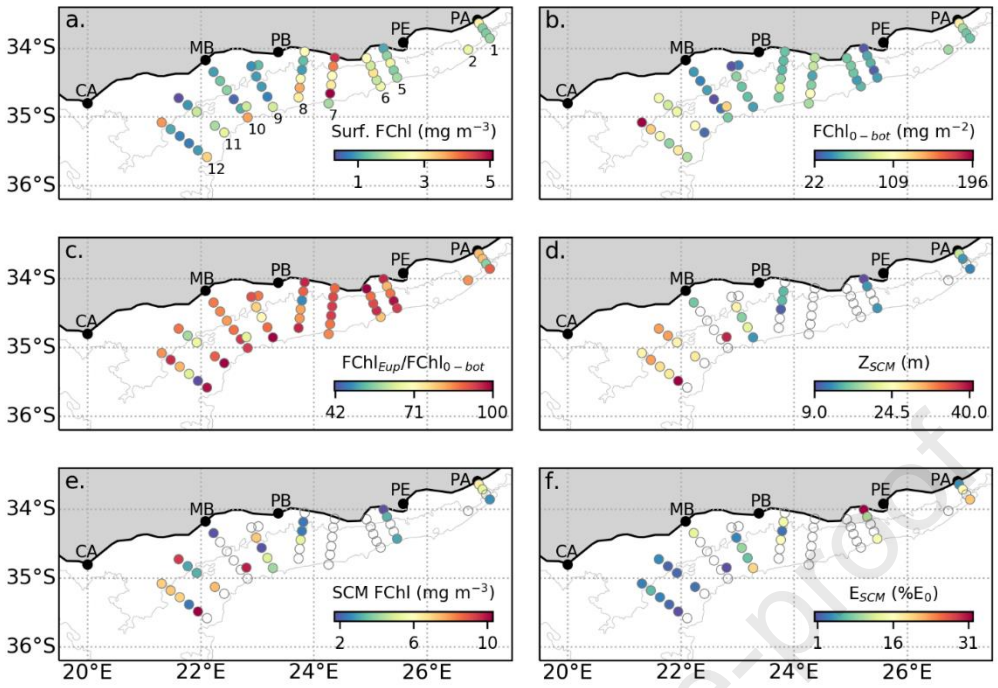

Figure 5.

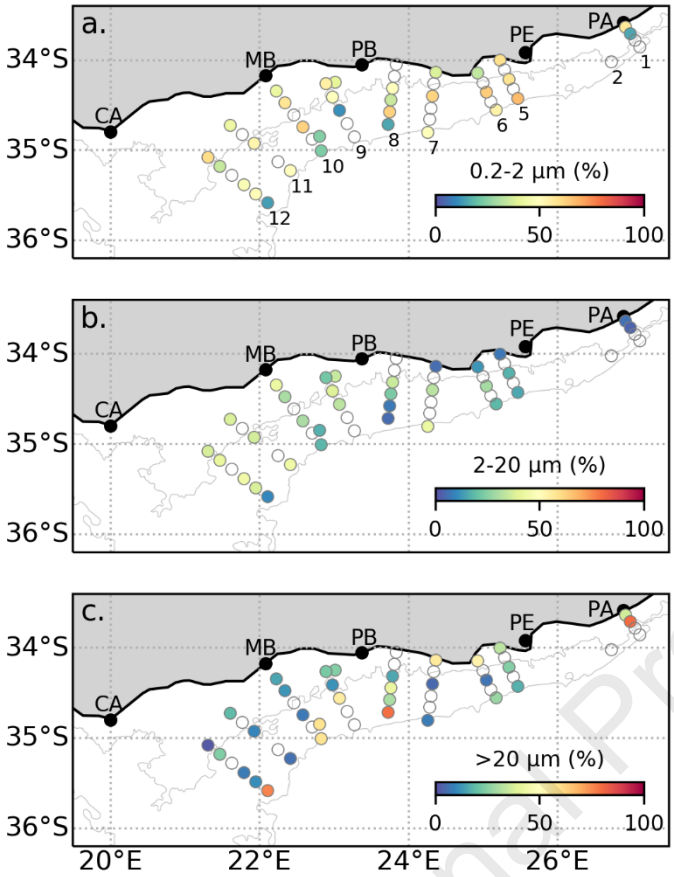

Figure 6.

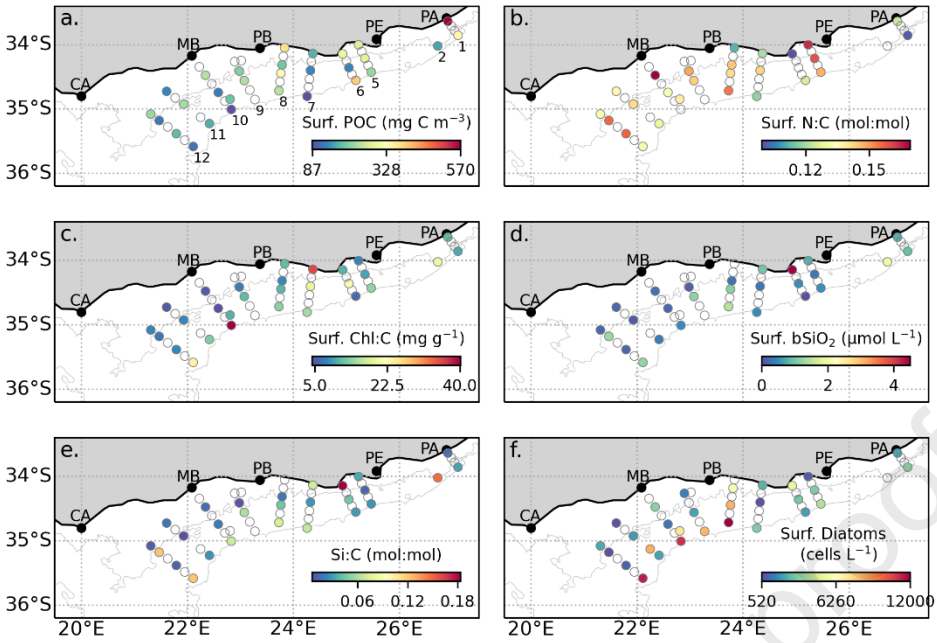

Figure 7

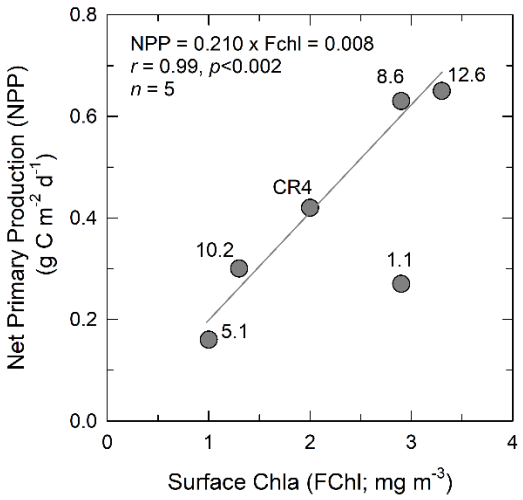

Figure 8.

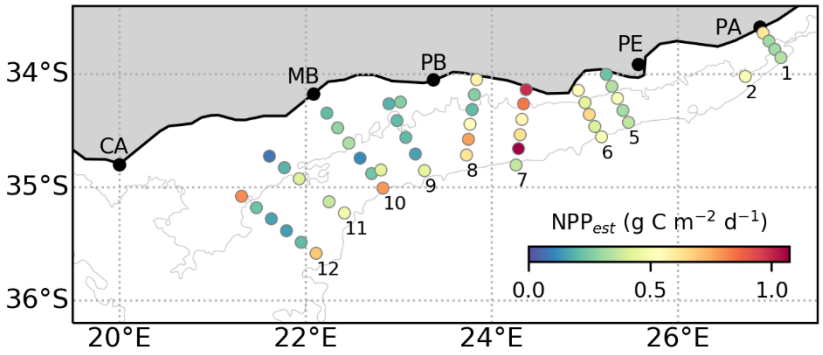

Figure 9.

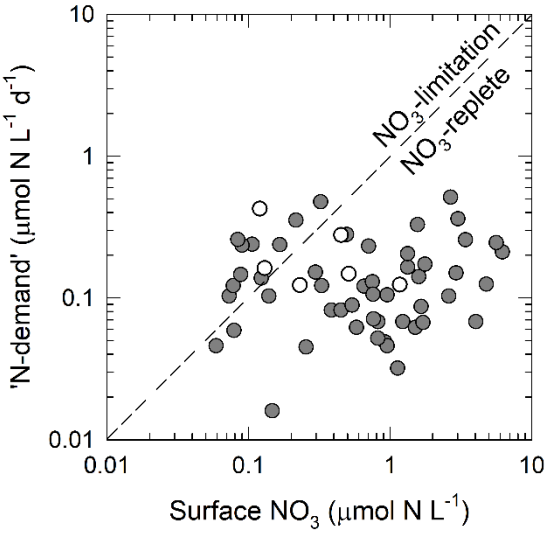

Supplementary Table S1.

Station ID	Lat.	Long.	SML $Si(OH)_4$ [µmol Si L^{-1}]	SML PO_4 [nmol P L^{-1}]	Surface particulate nitrogen (PN) [mg N m^{-3}]	SML average salinities	BML average temperature [ºC]	BML average salinity	BML PO_4 [nmol P L^{-1}]	BML $Si(OH)_4$ [µmol Si L^{-1}]
1.1	-33.64	26.92	2.5	219	71	35.26	13.4	35.24	1210	13.2
1.2	-33.71	26.98	0.8	120	ND	35.24	11.7	35.11	1160	10.3
1.3	-33.78	27.04	2.0	228	ND	35.38	11.1	35.05	1210	11.0
1.4	-33.86	27.11	1.4	192	35	35.37	10.1	34.95	1320	13.3
2.3	-34.02	26.73	2.4	316	ND	35.38	10.9	35.03	1240	11.4
5.1	-34.01	25.23	5.1	385	45	35.23	10.0	34.95	1600	20.6
5.2	-34.11	25.29	3.6	202	ND	35.29	9.9	34.93	1520	18.2
5.3	-34.22	25.35	3.4	209	44	35.32	9.1	34.86	1560	20.1
5.4	-34.32	25.41	3.7	399	ND	35.30	7.8	34.77	1800	26.8
5.5	-34.43	25.47	3.6	433	32	35.25	7.6	34.75	1850	29.3
6.5	-34.56	25.18	2.0	251	49	35.32	8.1	34.78	1710	23.2
6.4	-34.47	25.11	2.0	239	ND	35.30	8.0	34.77	1710	23.3
6.3	-34.36	25.05	3.5	348	ND	35.26	8.0	34.78	1730	24.9
6.2	-34.25	25.00	4.4	355	ND	35.31	9.2	34.87	1540	19.6
6.1	-34.15	24.93	4.2	298	29	35.27	13.0	35.04	1410	18.7
7.1	-34.14	24.37	3.5	343	21	35.22	10.0	34.95	2290	20.4
7.2	-34.27	24.34	4.9	378	ND	35.25	9.4	34.87	1440	15.8
7.3	-34.40	24.33	4.5	522	19	35.29	9.0	34.83	1460	15.5
7.4	-34.54	24.31	4.1	478	ND	35.29	9.3	34.86	1400	13.9
7.5	-34.66	24.29	3.2	303	ND	35.26	9.8	34.91	1340	12.9
7.6	-34.81	24.26	1.4	182	10	35.29	8.7	34.80	1510	16.9
8.6	-34.72	23.73	3.0	127	37	35.37	9.0	34.83	1480	15.6
8.5	-34.58	23.75	3.2	142	ND	35.36	9.7	34.89	1340	12.2
8.4	-34.45	23.77	3.1	109	45	35.33	9.8	34.92	1350	13.8
8.3	-34.32	23.79	3.6	147	28	35.35	9.7	34.92	1410	15.6
8.2	-34.18	23.81	3.7	161	ND	35.35	9.4	34.89	1500	17.8
8.1	-34.05	23.84	3.2	204	42	35.14	9.6	34.90	1600	20.0
9.1	-34.27	22.89	2.6	166	ND	35.27	10.1	34.95	1260	12.1
9.1	-34.27	22.90	2.8	206	ND	35.33	10.0	34.94	1450	16.0
9.2	-34.41	22.98	3.7	274	31	35.28	9.5	34.90	1470	17.3
9.3	-34.56	23.08	3.6	196	34	35.36	9.9	34.93	1350	13.4
9.4	-34.71	23.18	3.6	199	ND	35.38	9.7	34.91	1360	12.9
9.5	-34.86	23.28	3.4	208	ND	35.35	8.7	34.79	1510	15.7
10.6	-35.01	22.83	2.7	250	ND	35.33	8.8	34.80	1490	14.9
10.5	-34.88	22.71	3.3	206	ND	35.34	8.7	34.80	1360	12.8
10.4	-34.75	22.59	3.6	225	17	35.35	9.8	34.91	1360	13.3
10.3	-34.61	22.47	3.1	194	ND	35.28	9.6	34.90	1510	17.4
10.2	-34.48	22.35	3.3	191	41	35.24	9.9	34.94	ND	ND
10.1	-34.35	22.23	3.3	171	ND	35.27	9.9	34.93	1600	19.2
11.1	-34.73	21.61	2.0	126	18	35.37	10.1	34.94	1890	21.8
11.2	-34.83	21.77	1.5	105	ND	35.38	10.0	34.92	1930	23.1
11.3	-34.93	21.93	3.3	205	32	35.24	10.1	34.94	1540	17.8
11.5	-35.13	22.25	2.8	170	ND	35.37	9.5	34.88	1220	10.3
11.6	-35.23	22.42	2.2	263	22	35.34	9.8	34.90	1200	8.5
12.6	-35.59	22.11	0.7	163	16	35.43	11.2	35.06	1010	5.8
12.5	-35.49	21.95	2.0	266	ND	35.35	9.8	34.91	1270	10.8
12.4	-35.39	21.80	3.9	251	28	35.21	10.4	34.98	1360	14.9
12.3	-35.28	21.63	2.4	154	ND	35.27	9.7	34.91	1780	21.7
12.2	-35.18	21.47	0.6	115	19	35.31	9.8	34.92	1670	18.6
12.1	-35.08	21.31	2.7	145	29	35.17	10.1	34.95	1760	19.5
CR4	-34.87	22.70	2.7	163	26	35.36	10.5	34.99	1160	8.7

Supplementary Figure 1.

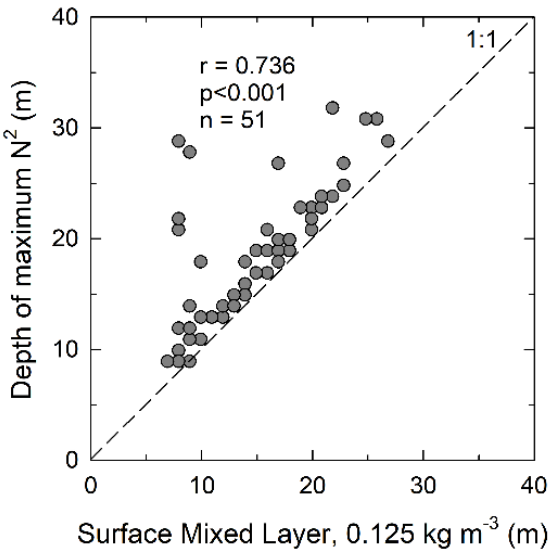

Supplementary Figure 2.

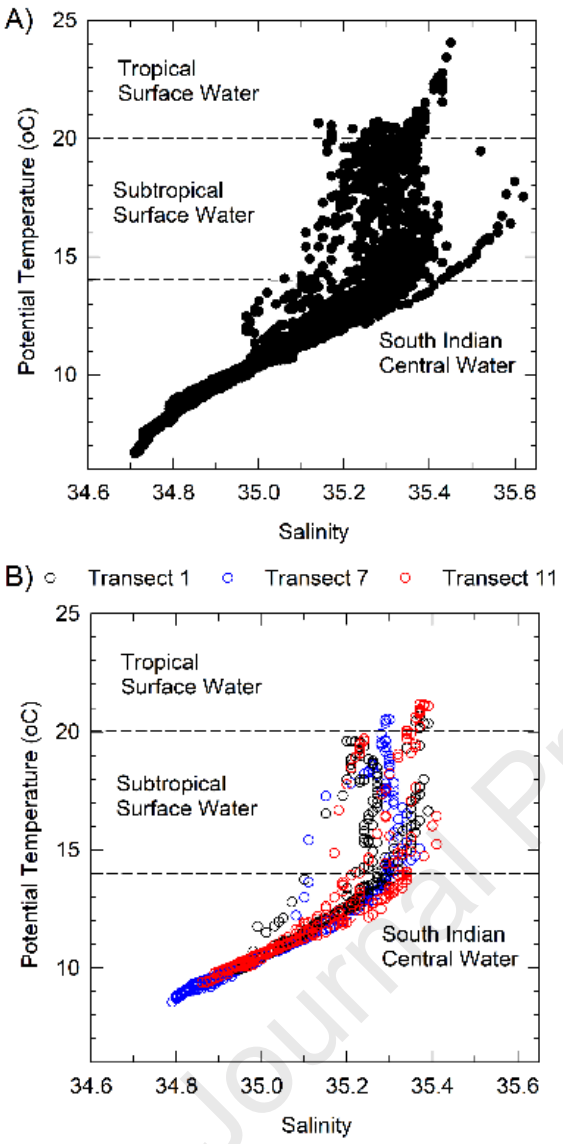

Supplementary Figure 3.

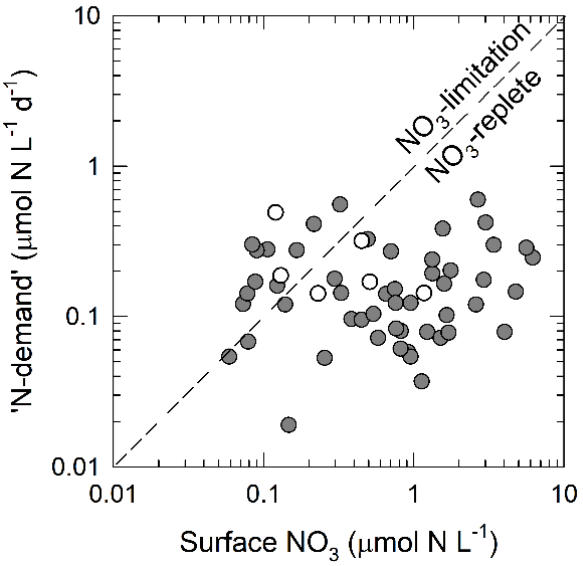

There are no conflicts of interest.